Magnetic tracing of fine-sediment over pool-riffle morphology

DAVID J. MILAN[1*] & ANDREW R.G. LARGE[2]

[1] *Department of Geography, Environment and Earth Sciences, University of Hull, Hull, HU6 7RX, UK, email d.milan@hull.ac.uk, tel +44 (0)1482 465570; fax +44 (0)1482 466340

[2] School of Geography and Politics, Daysh Building, Newcastle University, Newcastle upon Tyne, NE1 7RU, UK,

*corresponding author

Abstract

Field studies documenting fine-sediment (<2 mm) transport in gravel-bed rivers are rare. For the first time in a fluvial environment, a technique that enhances the magnetic susceptibility of sand is used to trace its longitudinal dispersion and storage. This paper describes the methodology behind the artificial magnetic enhancement of iron-stained sand, and presents the results from sand tracing exercises conducted on two gravel-bed channels with pool-riffle morphology; one unregulated and sinuous in nature (site A), the other regulated and straight (site B), both situated on the River Rede Northumberland, UK. Two tonnes of magnetically enhanced tracer sand was introduced to site A and four tonnes to site B, to provide information on fine-sediment storage dynamics, interaction of fines with the stream bed, and rates of movement, expressed as virtual velocity (V_i). Sand transport pathways appeared to differ between the reaches; for site A, sand storage was found on bars and riffle margins with no storage or signs of transport through pools, in contrast pool storage of tracer was a feature shown at site B. Topographic forcing may cause differences in sediment sorting at site A; topographic highs tend to have low sand transport rates with sand grains becoming congested in these areas, whereas topographic lows show higher transport rates resulting in greater dispersion. Supply limitation of sand on the falling limb of the hydrograph may also become an issue in the topographic lows at this site. Hydrograph differences between the regulated and unregulated reaches could also play a role, however this could not be quantified in this study. There was no evidence of sand infiltration into the bed at site A, however marginal evidence for infiltration into the near-surface (0-15 cm) substrate voids was found at site B. The general lack of evidence for significant infiltration may reflect limited availability of void space in substrate framework gravels. Tracer sand was transported over the bed surface, with little vertical interaction with the substrate, despite periods of gravel mobilisation at site A. V_i over the study duration for site A was 2.28 m day^{-1}, and 0.28 m day^{-1} for site B. These

values are greater than those calculated using existing predictive equations developed from gravel tracer data, possibly reflecting differences in the mode of transport between bedload and saltation load.

Key words: magnetic susceptibility, tracer, sediment-transport, pool-riffle, siltation

1. Introduction

Information regarding fine bedload (< 2 mm) transport in rivers is limited (e.g. Church et al., 1991), despite the significance of this grain-size class to the total sediment load, to instream biota such as salmonids, and macroinvertebrates (Milan et al., 2000; Kondolf et al., 2008; Jones et al., 2011), and it's association with toxic heavy minerals in contaminated river systems (Petts et al., 1989). Sand is predominantly transported as the saltation component of the bedload (Garde and Ranga Rangu, 1977), and its transport is complex due to its interaction with bed morphology and the gravel component of the bed substrate.

1.1 Fine-sediments and pool-riffle morphology

In gravel-bed streams displaying pool-riffle morphology, its longitudinal dispersion has been linked with tractive force variability over the flow regime (Lisle, 1979; Jackson and Beschta, 1982; MacVicar and Roy, 2011; de Almeida and Rodríguez, 2012). At low flow, fines may be stored surficially in areas of low tractive force such as pool exit slopes, channel margins, and in the lee of coarse clasts (Carling and Reader, 1982; Lisle and Hilton, 1992; 1999). Fines may also be stored in void spaces between framework clasts in the sub-surface sediments beneath the armour (Carling and Reader, 1982; Milan et al., 2000). On the rising limb of a flood, tractive force increases over both riffles and pools, and may flush surficial deposits stored in pools (Lisle, 1979). At higher discharges approaching bankfull, the armour layer on the riffles is mobilised, releasing the substrate framework gravel and interstitial fines, increasing sediment-transport rates (Reid et al., 1985). The rate of tractive force increase with discharge has been reported as being greater for pools compared with riffles and can equal or exceed adjacent riffles (Keller, 1971; Milan et al., 2001), leading to pool scour and riffle aggradation (Vetter, 2011; de Almeida and Rodríguez, 2012). On the falling limb of a flood, gravels are deposited initially, and then fines may be selectively transported across the bed surface and deposited in areas of low tractive force (e.g. pool exit slopes) (Lisle and Hilton, 1992; 1999; Vetter, 2011). These sediment-transport processes are thought to be responsible for the observed sediment-sorting differences commonly observed between pools and riffles; with pools most commonly being reported as being finer (Milan, 2013a). de Almeida and Rodríguez (2012) further highlight that the falling limb of the hydrograph is particularly important in re-establishing grain-size differences between pools and riffles that are lost at high flow.

1.2 Gravel-bed structure

Gravel-bed rivers tend to show a vertical variation in sediment structure; often having a fines-free coarse surface layer of grains known as an 'armour', 'pavement', or 'censored layer', and a finer sub-surface mixture of framework gravels, the voids of which are filled to varying degrees by a matrix of fines (< 2 mm). The terms 'armour' and 'pavement' have been used interchangeably by different workers, either to describe single-grained surface layers that experience regular disruption during floods, for example those under 'natural' hydrological and sediment supply regimes, or static surface layers found where the flow hydrograph and sediment regime has been altered, such as downstream of dams (Bray and Church, 1980; Parker et al., 1982; Sear, 1995). The term 'mobile' armour and 'static armour have also been used to describe these two situations, and is adopted in this paper (Sutherland, 1987; Powell, 1988). Censored layers present a third class of surface layer that are greater than one grain thick, comprise and open-work structure (Carling and Reader, 1982), and can be a feature of regulated gravel-beds below dams (Wyżga, 1993). Although there are some differing explanations for surface coarsening (Richards and Clifford, 1991), it is generally accepted that the bed surface becomes coarser after selective removal of fines, transported downstream across the bed surface into areas of lower tractive force, and infiltration into void spaces in the underlying framework gravels.

1.3 Infiltration mechanisms

Infiltration of fines into available interstitial voids can follow one of two styles; filling from the base upwards (Einstein, 1968), or bridging of near-surface voids between the framework gravels (Beschta and Jackson, 1979). The style of infiltration is dependent upon the size of the incoming fine-sediment and the size and shape of the receiving void spaces (Frostick et al., 1984). Scour and fill of the channel bed also influences the interstitial fine-sediment (matrix) component of the bed, through re-exposing infiltrated material or burying previously infiltrated fines (Lisle, 1989). The majority of studies that have monitored fine-sediment infiltration have been based in the laboratory and have used openwork gravels as the start point (e.g. Einstein, 1968; Beschta and Jackson, 1979; Carling, 1984; Schälchli, 1995). Field studies have usually used traps; e.g. empty solid walled traps (Church et al., 1991), or porous traps filled with openwork gravel (e.g. Sear, 1993; Acornley and Sear, 1999). Few studies have investigated infiltration of fines into an undisturbed river bed.

1.4 Influence of flow regulation

In regulated rivers the flow hydrograph may be altered in a number of different ways depending upon the operation of the dam (Petts, 1984), however discharge magnitude and frequency are usually reduced (Williams and Wolman, 1984). Gravel supply is completely shut off, yet fine organic-rich sediments may be delivered to the channel downstream (Meade and Parker, 1985; Gilvear, 1988; Sear, 1995; Vericat and Batalla, 2005). Modified flow and sediment supply disrupts quasi-equilibrium within the channel, and channel responds through altering its form and sedimentology (Brandt, 2000). The exact nature of channel response is dependent upon the nature of flow (e.g. hydrograph peak and shape) and sediment supply alteration, and generally decreases in magnitude with distance from the dam (Petts, 1979; Petts and Gurnell, 2005). Typically for the channel immediately downstream of the dam and upstream of the first major non-regulated tributary junction, reduced discharges are generally unable to mobilise the coarser gravels. (Wyżga, 1993; Sear, 1995). However flows are usually capable of selective removal of the finer fractions, resulting in bed degradation, and surface coarsening (Galay, 1993; Sear, 1995; Fasnnacht et al., 2003). Occasionally, wash-out of interstitial fines occurs more deeply into the sub-surface resulting in an openwork or censored surface layer (Wyżga, 1993). However, sub-surface gravels have also been reported to experience enhanced siltation in some instances (e.g. Petts, 1988; Sear, 1995). The pool-riffle bedform can also show a response to modified flow and sediment-transport regimes caused by flow regulation. In Sear's (1995) study on the river North Tyne, UK, riffles showed degradation and pools aggradation, in response to hydropower releases. de Almeida and Rodríguez (2012) further support Sear (1995), indicating that the reservoirs operating increased duration of low to medium discharges, with a reduction of peak flows, may cause significant degradation of pool-riffle morphology, and reduce sorting contrasts between pools and riffles.

1.5 Step-length data

A knowledge of transport distance (step-length) for different grain-size fractions is required in the calculation of sediment-transport rates, knowing the width and depth of the active layer (e.g. Haschenburger and Church, 1998), to improve understanding of sediment dispersion dynamics (Ferguson and Wathen, 2008; Hashenburger, 2011; Milan 2013b). Despite its significant contribution to the total sediment load in gravel-bed rivers; sub-surface sediments in England typically contain between 15 and 48% < 2 mm material (Milan et al., 2000). Step-length data for the saltation load are not usually accounted for, despite known differences in size-based competence duration.

This paper aims to:

1) Explore spatial patterns of sand sorting over pool-riffle topography;
2) Examine sand infiltration into an undisturbed gravel-bed;
3) Contrast fine-sediment-transport and infiltration processes in an unregulated and regulated channel;
4) Provide step-length data for a series of flood events for the sand fraction.

2. Field location

The study focused on two 400 m reaches on the River Rede, Northumberland, UK, an upland gravel-bed stream (Fig. 1). The Rede has a Strahler order of four, and has its source area in the Cheviot Hills at 490 m above ordnance datum (defined as mean sea level at Newlyn, Cornwall UK). The study reaches were selected on the basis of one having a near-natural flow regime and a mobile armour (site A), and the other having a regulated-flow regime and static armour (site B).   One of the reaches (site A) is sinuous (sinuosity = 1.7), and the other (site B) is straight (sinuosity = 1.1). Both sites had well-defined sequences of pools and riffles and were located 4.5 km and 7.5 km from the source of the river, having catchment areas of 18 km^2 and 41 km^2, respectively (Fig. 1A). A mean annual rainfall is 1026 mm, falls on to a catchment underlain by an impermeable geology of Carboniferous sandstones and shales, overlain by peat and till. Continuous stage was recorded at site A over the study duration, and converted to discharge using a rating relation (Fig. 2). Continuous stage was not available for site B, so discharge peaks for the flood events between survey dates were estimated using the Manning formulae, where hydraulic radius was calculated from trash-line observations surveyed relative to a fixed cross-section at the head of the reach. Site A (55° 19.942′ N., 2° 26.457′ W.) is unregulated and experiences a flashy hydrological regime (with a bankfull discharge of 8.5 m^3s^{-1}), whilst Site B (55° 19.308′ N., 2° 23.573′ W.) has been regulated since 1905 by the Catcleugh reservoir. Catcleugh reservoir is used for water supply, and the hydrological regime immediately downstream consist of extended periods of low 'compensation' discharges of 0.16 m^3 s^{-1}. Occasional floods overtop a spill-weir during the winter months, with bankfull discharge equating to 29 m^3 s^{-1}. During this investigation flows remained at the compensation discharge until 12th November 1996. Elevated flows were experienced during the rest of the investigation, through to April 1997, due to overflow of the Catcleugh spill-weir. The morphological impacts of flow regulation at site B were highlighted by Petts (1979), and include channel degradation, enhanced armouring limiting further scour, and increased width:depth ratio in response to bank erosion.

Figure 1 Study location A) Rede catchment, B) site A, C) site B. Magnetically enhanced sand was seeded at the upstream end of each reach, as indicated by the grey boxes. The approximate extent of pools (P), riffles (R), and bars (B) are highlighted. Flow direction is indicated by the arrow. Position of basket and grab samples are highlighted as red points.

Figure 2 Discharge hydrograph over the study duration recorded at Site A. Green arrow indicates date of tracer seeding, red arrows indicate sediment sampling dates.

3. Methodology

3.1 Tracing fine-sediment

This study employed sediment tracing to explore sand-transport dynamics. Previous studies have used radioactivity (Crickmore, 1967; Hubbel and Sayre, 1978), fluorescence (Rathburn and Kennedy, 1978), exotics such as limestone (Moseley, 1978) and heavy minerals such as cassiterite (Hughes, 1992) or pure magnetite (Carling et al., 2006) to trace fines in fluvial systems. However, problems are encountered with most of these methods. Radioactively enhanced fines may be toxic to aquatic life, whilst exotics and heavy minerals have a higher density compared with river sediment and thus have different transport dynamics. Rummery et al. (1979), Arkell (1985), Arkell et al. (1983), and Sear (1996) have all demonstrated the application of artificially enhanced iron-rich bedload to trace coarse bedload through fluvial systems. van der Post et al. (1994) have demonstrated the application of artificially magnetically-enhanced sand for detecting tidal induced movement of beach sands. For the first time this study applies the van der Post et al. (1994) approach to a fluvial environment.

3.2 Tracer manufacture

The van der Post et al. (1994) methodology is a modification of the techniques originally developed by Rummery et al. (1979), Arkell (1985), Oldfield et al. (1981) and Arkell et al. (1983). By heating iron-rich sediments the apparent in-phase magnetic susceptibility (χ) is enhanced. The enhancement process is dependent upon the degree to which the red coloured iron-oxide coatings on the outside of the material being used (in this case silica sand grains) can be converted into magnetite (black coloured) / maghaemite (pink coloured). Iron-stained (red) sands are available in a number of locations in the UK, including glacial-outwash deposits derived from Triassic rocks in North Wales, Cheshire and Shropshire, and from the Cretaceous "Greensand" quarries in Bedfordshire, UK. The process of magnetic enhancement involves toasting the sand at high temperatures (~ 700^{o}C) for two hours in a reducing atmosphere (achieved by mixing flour into the sand), followed by rapid cooling in air. A series of pilot laboratory experiments were conducted on small (10 g) samples to identify the degree of enhancement, and the optimum conditions for enhancement. Fig. 3A illustrates the degree of enhancement in a range of potentially suitable sands. Maximum enhancement was identified for 'Greensand', obtained from Potton, Bedfordshire, where values of mass susceptibility (χ_t) ranged from 177 to 190 × 10^{-7} m^3 kg^{-1}. Bedfordshire Greensand was then used to test for the effects of temperature, atmosphere (i.e. organic flour concentration), and period of heating. The results are demonstrated in Figs. 3 B-D where it can be seen that the optimum temperature was between 600 and 700^{o}C. The concentration of organic material used to control atmosphere did not appear overly critical, with low concentrations (1 part in 40 to 1 part in 5) being slightly more favourable. The duration of heating also did not appear to be a critical factor.

In the field-tracing experiment, six tonnes of Bedfordshire Greensand was mixed with one tonne of flour (reducing agent), and toasted for three hours at 700^{o}C. The sand-flour mixture was loaded into large tins and mounted on a trolley, which was then placed into a large commercial brick-firing kiln at Redland Bricks Ltd, Throckley, Newcastle upon Tyne, UK (Fig. 4A).

Figure 3 Results of laboratory trials into the optimum conditions for magnetic enhancement, A) Comparison of enhanced tracer sands and background samples taken from the Rede site, B) effect of temperature, C) influence of heating duration at 700°C, D) influence of reducing agent concentration

Figure 4 Sand tracing experiment, A) Magnetic enhancement of iron stained sand: sand-flour mixture was placed in large tins and roasted in the 'specials kiln' at Redland Brick Works, Newcastle upon Tyne, B) introduction of magnetic sand to the channel at site B, C) raking sand over the bed surface at site A, D) back coloured magnetic sand on the pool bed at site B shortly after introduction, E) deposition on the edge and surface of point bar 3 at site A, F) close-up of surface deposition on the edge of bar 3 at site A.

3.3 Tracer deployment

The quantity of tracer required is likely to vary significantly depending upon the size of the channel and flow regime. The quantity of tracer introduced by other workers in similar studies has varied significantly. For example Sear (1996) introduced just 230 kg of magnetically enhanced gravels to the 35 m wide regulated North Tyne, where flood peaks of up to 151 m^3s^{-1} were experienced during the study (Sear, 1992). Carling et al. (2006) introduced 20 tonnes of magnetite to a gravel bar on the River Severn at Dolhafren, Powys, Wales (bankfull discharge of 95 m^3s^{-1}). The quantity of sand introduced to the study sites in this study was partly controlled by the maximum quantity that could be toasted in a single firing in a brick kiln, and the logistics of transporting the magnetically enhanced sand to the channel. However, the quantities used were approximately one-tenth of those used by Carling (2006), and scaled well with the bankfull discharge at the Rede sites. Magnetically enhanced tracer sand was delivered to the seeding location at site A across 600 m of boggy terrain, using a team of volunteers, whereas vehicular access to the seeding point at site B was available. Once delivered to each site, the tracer was seeded on to the stream bed in a 12 × 6 m area located upstream of a pools at both sites (Fig. 1B and C, Fig. 4D). A total of 2326 kg (dry weight) of sand was introduced by hand to the channel at site A during low flow conditions (0.23 m^3s^{-1}) on 20 April 1996, whilst 4000 kg was introduced to site B using tractor, on 13th June 1996 (Fig. 4C and D).

In order for the first tracer movement to be considered in the analysis, it was important for the tracer to be positioned into a “natural” position on the bed. With gravel tracer studies, the first movement is often not included in the analysis as the tracer grains may be over-loose and move further compared to tracers incorporated into the bed structure. However fine-sediments are often reported as being stored loosely on the bed surface; for example Lisle and Hilton (1992; 1999) report low flow storage of sand on the bed surface of pool troughs and exit slopes. The seeding strategy used in this study thus attempted to mimic this pattern; with magnetic sand introduced to a pool at the head of the study reaches during a low flow period. During the seeding operation, sand-sized grains *ca*. >63 μm settled onto the bed with no visible downstream dispersion during the seeding operation, whilst some of the finer grades (ca. <63 μm) were transported in suspension. Once on the bed, the sand was spread evenly over the bed of the pool troughs and exit slope using a rake (Fig. 4C).

3.4 Basket trapping

To detect movement of tracer on an event-by-event basis, 33 sediment traps were placed on riffles and pools at site A (Fig. 1B). Forty traps were located at site B, predominantly on pools and riffles *ca*. 100 m downstream of the seeding location (Fig. 1C), but also at various points downstream up to *ca*. 400 m downstream of the seeding location. The traps, based on the design used by Sear (1993) were 15 cm deep, with a surface area of 314 cm^2 and a capacity of 4710 cm^3 (Fig. 5A). Each basket was constructed from 10-mm wire mesh to allow intragravel flow. To assist efficient retrieval of trapped fines, a compressed bag with a wire rim was folded and placed at the base of the basket and connected to the surface with cables to enable removal when full (Fig. 5). Baskets were pre-filled with representative sub-surface framework gravel truncated at 2 mm. The armour layer was reconstructed over each basket once it had been set within the streambed using painted clasts from the local vicinity. On sampling, these clasts were removed and the compressed plastic bag was then pulled upwards via the cables in order to minimise loss of fines under flowing water. The framework and accumulated fines mixture retained within the bag were then wet sieved through a 2 mm sieve in the field and organics floated off in a bucket. Traps were re-set using the cleaned framework material and armour clasts replaced, and the sampling repeated 14 times over a 12 month period for site A, and 6 times over a 9 month period for site B. Grab-samples of fines were also taken from the bed surface along the channel margins for up to 400 m downstream of the seeded zone.

Figure 5 Fine-sediment sampling, A) Basket trapping, B) Freeze-coring

3.5 Freeze-coring and background magnetic susceptibility

To allow detection of tracer infiltration into the undisturbed bed, liquid nitrogen freeze-cores (Milan, 1996) were taken from riffles at site A (Fig. 5B), prior to the introduction of tracer in July 1996 (80 cores), and after the first event causing tracer movement in June 1996 (27 cores). Freeze-cores (86 Cores) were taken from Site B during July 1996, to establish background χ_t of matrix sediments, and in March 1997, nine months after seeding. Freeze-cores were sectioned at 15 cm intervals, dried and sieved for grain-size analysis, and the < 2 mm fraction retained for magnetic analysis.

Fine-sediment (< 2 mm) samples taken from basket traps, freeze-cores and grab samples were oven dried at 40ºC, and weighed to establish average accumulation rates following each event. Measurements were made on 10 ml sub-samples of < 2 mm material using a laboratory-based magnetic susceptibility instrument, calibrated against known standards before each individual measurement (Stephenson and de Sa, 1970), allowing mass susceptibility (χ_t) to be obtained with units of measurement in m^3 kg^{-1}. It was important to establish the natural background χ_t, so that the tracer could be detected. Magnetic susceptibility measurements were made on samples of < 2 mm sediments derived from sectioned freeze-cores at both sites. The population of χ_t values for background samples taken from each site is shown in Fig. 6. Mean and maximum background χ_t for Site A was 3.9×10^{-7} m^3 kg^{-1} and 11.1×10^{-7} m^3 kg^{-1} respectively ($\sigma = 1.72 \times 10^{-7}$, n = 99), and for Site B 4.9×10^{-7} m^3 kg^{-1} and 12.2×10^{-7} m^3 kg^{-1} ($\sigma = 2.18 \times 10^{-7}$, n = 122). The threshold level of detection was taken to be the maximum χ_t background values for each site.

Figure 6. Background χ_t distribution for matrix sediments sampled at sites A and B.

4. Results

4.1 Grain and void size

Fig. 7A demonstrates the grain-size distributions for the armour layer sampled using a Wolman (1954) grid strategy, where the intermediate axis of 100 clasts were randomly measured from each riffle in both reaches, and the sub-surface framework sediments sampled using freeze-coring. The armour D_{50} of the riffles at site A was 85 mm, and at Site B was 74 mm. The framework D_{50} values were 46 mm for Site A and 66 mm for site B. Morphological re-survey and tracer investigation at site A indicates that gravel mobilisation is initiated at 1.8 m^{3}s^{-1}, and that transport is patchy in nature (Milan et al., 2001; 2002). Although gravel mobilisation and resurvey information is unavailable for site B, it is thought that the armour is ‘static’ in nature due to the long period of flow regulation where stream power is no longer competent to mobilise the coarsest material in the bed (Petts, 1979). This is further evidenced by moss-covered boulders and cobbles on the bed surface. Grain-size information for the matrix component of the sub-surface sediments, and the tracer sediment (Bedfordshire Greensand, Potton) both prior and post enhancement, and the initial grain-size distribution of the void spaces in the armour layers on the surface of the traps is also demonstrated (Fig. 7B). The initial D_{50} for void spaces was 12 mm for site A and 10 mm for site B. The D_{50} for the matrix sediment at site A was 0.38 mm and 0.41 mm for site B. The grain-size of the introduced-tracer material demonstrate the pre-enhanced sand to be slightly finer (D_{50} = 0.73) than the post-enhanced material (D_{50} = 0.78).

Figure 7 Cumulative grain-size information for the river Rede, A) Armour and framework grain-size distribution for sites A and B, B) void, matrix, unenhanced and magnetically enhanced sand grain-size distributions.

4.2 Accumulation rate of fine-sediment

The average rate of accumulation in the basket traps at each site against the previous peak discharge is shown in Fig. 8. A clear relationship between flow magnitude and fine-sediment accumulation is evident for both sites. Solid symbols in Fig. 8a for site A indicate periods when χ_t values were in exceedance of the natural background at the site; hence sediment accumulating in the traps contained the tracer. Open symbols show accumulation rates where no tracer was detected within the samples accumulating in traps. Accumulation rates do not appear to be significantly higher during periods when tracer is detectable within the system, compared to accumulation rates unaffected by tracer introduction. The relationship between flow and accumulation at Site B, shows a peak in accumulation rate after a peak discharge of 6.4 m^3s^{-1}, earlier on in sampling, rather than the peak flow of 14.4 m^3s^{-1} at the end of the sampling period (Fig. 8b). This may reflect partial exhaustion of tracer, and starvation of natural fine-sediment supply by the Catcleugh dam.

Figure 8 Relationship between mean sediment accumulation (based upon 31 traps at each site) and discharge for a) site A, and b) site B. Closed symbols represent periods where magnetic tracer was detectable within the system.

Sediment accumulation rate data for the unregulated site A can be used as a cross-check on the quantity of tracer introduced to each site. The rating relation shown in Fig. 8A for site A, predicts 0.85 kg m^2 d^{-1} of deposition at bankfull discharge (8.5 m^{3}s^{-1}). This is equivalent to 2071.45 kg of sand spread over the 2437 m^2 reach area shown in Fig. 1b, close to the mass of the tracer seeded at this site. Application of the site A rating relation to the regulated site B, using a bankfull discharge of 29 m^{3}s^{-1}, predicts an accumulation rate of 2.457 kg m^2. A total of 3686 kg of sand would have been deposited over a reach area of 1500 m^2 (for the first 100 m length of this study site shown in Fig. 1c. The quantities of tracer introduced to each site were therefore appropriate.

4.3 Sand sorting over pool-riffle morphology

Spatial patterns in χ_t for the upstream 250 m of each reach before and after tracer emplacement are shown as contour plots (Fig. 9 and 10). Contour plots were produced using Golden Software Surfer, using universal kriging to interpolate χ_t values on a 1 m grid. Kriging is appropriate for irregularly spaced data, and has been used in a number of fluvial studies to model morphological data (e.g. Fuller et al., 2003; Heritage et al., 2009). Contour plots for three surveys are presented for site A, where greater spatial coverage of χ_t data was available; including basket trap data and grab samples. Five surveys are presented for site B, based upon lower spatial resolution basket trap data alone. The mean and range of χ_t values used to create each contour plot is presented in Table 1. Interpolation error, calculated as the difference between the measured points and the interpolated surface, is also highlighted alongside. Greater error is apparent for the contour plots produced for site B, due to the lower point density. However errors are still relatively low considering the mean and range of χ_t values used to generate the plots.

Figure 9 Spatial patterns of magnetic susceptibility of fine-sediments deposited over pool-riffle morphology at site A, A) Background characteristics, B) magnetic susceptibility on 30th April 1996, one week after tracer emplacement following a peak discharge of 0.5 m^{3}s^{-1}, and C) magnetic susceptibility on 22nd May 1996, following a 3.6 m^{3}s^{-1} event.

Figure 10 Spatial patterns of magnetic susceptibility of fine-sediments deposited over pool-riffle morphology at site B, A) Characteristics immediately following tracer emplacement on 13th June 1996, indicating background conditions, magnetic susceptibility on B) 2nd Nov 1996 following a steady discharge of 0.16 m^3s^{-1}, C) 12th Nov 1996, following a peak flow of 11.0 m^3s^{-1}, D) 23rd Dec 1996,, following a peak discharge of11.9 m^3s^{-1}, E) 11th March 1997, following a peak discharge of 14.4 m^3s^{-1}.

Table 1 Mean and range of χ_t values, and interpolation error for the contour plots (Figs. 9 and 10), recorded at each site over the study period

Data for one week after emplacement of tracer at site A indicate highest values to be found in the top pool (1) indicating the location and extent of the seeded zone (Fig. 9B). A small amount of redistribution took place under low flow conditions (< 0.5 m^3s^{-1}), where occasional high χ_t values were observed on riffle 1 downstream of the seeded zone, reflecting selective transport from the tail of the pool onto the riffle and towards the tail of bar 2. Much greater re-distribution is demonstrated after the survey taken on the 22 May 1996, which followed a flood peak of 3.2 m^3s^{-1} (Fig. 9C), where partial exhaustion of the seeded zone was observed. The contour diagram (Fig. 9C) coupled with field observation, indicated that most of the tracer had been deposited on bar surfaces and on riffle margins. Patches of the black coloured tracer were clearly observed on bar surfaces and wake deposits behind coarse clasts (Fig. 4E and F). Greatest concentrations of tracer appeared to be deposited on a point bar located 90 m downstream of the seeded area (Bar 3; Fig. 4E, 9C).

The first contour plot for site B (Fig. 10A) undertaken five months after tracer seeding, indicates some selective transport from the seeded pool tail along the right-hand side of riffle 1; a higher energy zone. The second contour plot in the series (Fig. 10B) shows further movement of the tracer under the compensation discharge; across the right-side of riffle 1 and through the right-side of pool 2. This selective transport took place during compensation flows (0.16 m^3s^{-1}). More significant redistribution took place after Catcleugh spill weir overtopped in November 1996. Fig. 10C shows the spatial distribution of tracer following an estimated flood peak of 11 m^3s^{-1}. Slightly lower values of χ_t are found in the seeded zone and highest concentrations are found on the right of riffle 1 and entrance to pool 2 (left bank). Increased concentrations are also evident in pool 3 and the head of riffle 3. Substantial redistribution is evident after an estimated flood peak of 11.9 m^3s^{-1} (Fig. 10D). The three riffles all show higher concentrations than the pools; with greatest concentrations still appearing on the left-side of riffle 1, although tracer is detectable in all pools. The final contour plot, following an estimated discharge of 14.4 m^3s^{-1}, appears to show exhaustion of the seeded zone, with χ_t concentrations returning to background levels (Fig. 10E). χ_t concentrations have reduced throughout the study reach, however greatest concentrations are still located towards the left-hand side of riffle 1, and in pool 2. Riffle 3 shows lower χ_t concentrations in comparison to pools 3 and 4. Overall the data do show differences to site A; fine-sediment does appear to be routed through the pools at this site and fines are occasionally deposited in the pools.

Clear spatial patterns were evident in the deposition of the tracer at both sites. An assessment of longitudinal dispersion of the tracer wave is needed to provide information on transport dynamics over time, and to estimate step-length and virtual velocity of the tracer.

4.4 Longitudinal dispersion

By measuring the χ_t of sand collecting in basket traps along the centreline of the channel, surficial deposits in the channel and on channel margins, and on bar surfaces at intervals downstream from the seeded zones, it was possible to monitor downstream progression of the tracer wave. Event-based longitudinal variations in χ_t are demonstrated in Fig. 11 for site A and Fig. 12 for site B. Each of these Figures is separated into two parts, so that the detail in downstream patterns can be observed more clearly. Both examples show dispersive wave behaviour; with site A being dispersed more rapidly in comparison to Site B probably due to the naturally variable flow regime. For site B, the tracer wave shows negligible development under a compensation discharge of 0.16 m^3s^{-1} (between June and November 1996). However, a much more significant response is shown during a period of winter high flows due to the Catcleugh spill weir overflowing. The tracer wave appears to be 'lumpy' in nature for both sites, possibly reflecting spatial variations in deposition shown in the contour plots (Fig. 9 and 10).

Figure 11 Downstream magnetic susceptibility waveform following different flow events for site A.

Figure 12 Downstream magnetic susceptibility waveform following different flow events for site B.

A mathematical expression of tracer movement based upon a spatial-integration technique (Crickmore, 1967; Arkell, 1985; Sear, 1996) allows the point at which the concentration of magnetic tracer is equal upstream and downstream, the centroid, to be calculated for successive flows. The position of the centroid reflects the subtleties of tracer release and dispersion. The centroid position (P_t), at time t, may be calculated from

$$P_t = \frac{x_i S_i}{S_i} \qquad (1)$$

where x_i is the distance downstream of the emplacement site at which a given tracer concentration S_i is found. Tables 2 and 3 demonstrated centroid progression over the study period for sites A and B respectively. A general trend of downstream centroid progression is evident at both sites with an average rate of movement of 0.62 m day^{-1} between 20th April 1996 and 11th March 1997 for site A and 0.28 m day^{-1} for site B between 13th June 1996 and 11th March 1997, when taking into consideration calendar time. The virtual rate of travel, which takes into consideration only the period when < 2 mm material was mobile (flows > 0.35 m^3s^{-1} for site A; > 0.16 m^3s^{-1} for site B, equated to a velocity of 2.28 m day^{-1} for site A and 0.28 m day^{-1} for site B).

Table 2 A flood-by-flood account of the tracer position though the Rede riffle-pool sequence for Site A

Table 3 A flood-by-flood account of the tracer position though the Rede riffle-pool sequence for Site B

Detection of the tracer against the natural background becomes questionable after the sixth event in the series (7.1 m^3s^{-1}). This coincides with negative movement of the tracer centroid of 6 m. Other more pronounced negative movements in the order of 20 m shown later on in the series, however χ_t values are below detection limits, hence should be discounted.

4.4.1 Comparison of transport distance and virtual velocity with existing prediction equations

Event-based transport distance and virtual velocity for gravels has been shown to relate to grain-size in a number of investigations (Church and Hassan, 1992; Ferguson and Wathen, 1998; Milan, 2013b). The relationship for the Rede developed using tracer gravels at site A (Milan, 2013b) is

$$log\, L^{*} = \text{-}0137\, D_s^{*} + 0.399$$

(2)

where L^* is the scaled transport distance $\frac{L_i}{L_{50}}$÷, where L_i is the average transport distance for the tracer and L_{50} is the average transport distance for the fraction containing the median grain-size of the surface sediments. D_s^* is the scaled grain-size $\frac{D_i}{D_{50s}}$÷, where D_i is the tracer grain-size, and D_{50s} is the median sub-surface grain-size (following Church and Hassan, 1992). This formula predicts event-based travel distances of 8.3 m and 4.5 m on average for sites A and B respectively, falling substantially short of the actual average travel distance per event of 16. 8 m for site A and 12.7 m for site B.

Rede tracer gravel virtual velocity in its dimensionless form (V^*) also shows a dependence upon grain-size

$$V^* = 94.818D^{*2.021}$$

(3)

where V^* is dimensionless virtual velocity $\frac{V_i}{\sqrt{gD_i}}$÷, V_i is the virtual velocity and g is acceleration due to gravity. This formula predicts a V_i of 0.74 m d^{-1} and 0.36 m d^{-1} respectively for sites A and B, for 2 mm material, close to the actual V_i values calculated using centroid data and calendar time, however under predicting V_i calculated using mobilisation period. Any under prediction may reflect differences in the mode of transport of material of this size class compared with gravels, with a dominance of saltation and suspension of the material, rather than bedload.

4.5 Infiltration of the tracer

Vertical variability in χ_t for background samples and after emplacement of the tracer and subsequent transport are demonstrated in the box and whisker plots in Fig. 13. For site A, there is a general trend for background χ_t to increase with depth, which is not shown for site B. Post introduction, infiltration of the tracer does not appear to be detected at site A. Although the median χ_t values were higher following introduction of the tracer (Fig. 13B), values did not exceed the threshold for detection (indicated as red stippled lines on Fig 13). No infiltration occurred despite gravel transport (bed disruption) at site A (see Milan et al., 2001), suggesting that sand moved over the bed surface, and that deeper void space may not have been available between sub-surface framework clasts. Small amounts of infiltration in the near-surface (0-15 cm) framework voids were detected at site B.

Figure 13 Vertical distribution in magnetic susceptibility of < 2 mm samples taken from freeze-cores, A) background values before introduction of the tracer at site A, B) values after the first flow responsible for movement of the tracer 3.2 m^3s^{-1}, sampled in June 1996 at site A, C) background values before introduction of the tracer at site B, D) values after a series of high winter flows peaking at 14.4 m^3s^{-1}, sampled in March 1997 at site B. Levels of detection are indicated by the dashed red lines.

5. Discussion

The fine-sediment tracing technique discussed in this paper may be used to provide data concerning (i) fine-sediment sorting, (ii) infiltration, and (iii) distance of transport.

5.1 Fine-sediment sorting

Negligible amounts of fine-sediment appeared to be deposited in pools at site A, as pool traps contained very little of the tracer material and the pool-bed surface appeared free of fines. Fine-sediments were almost exclusively deposited and stored on morphological high points, particularly two point bars within the upstream 250 m of the reach. Most of this material was stored on the surface on the bar, rather than penetrating gravel framework voids. The riffle armour along the thalweg tended to be clean of fines, probably due to re-distribution into areas of lower energy, although there was some deposition on riffle margins. These data were somewhat different from the expected pattern. It had been anticipated at the outset of the study that the pools would fill with excess tracer under winnowing flows on the falling limb of the hydrograph (*sensu* Lisle and Hilton, 1992). In contrast, traps in pools at site B did collect some of the tracer material, occasionally showing higher concentrations than the riffles.

5.1.1 Effects of flow and sediment-transport regime upon sorting

Hydrograph character and sediment supply is known to influence pool-riffle sediment-transport processes and maintenance (Sear, 1995; de Almeida and Rodríguez, 2012). de Almeida and Rodríguez (2012) suggest that a variable hydrograph regime, like that shown at site A, should produce sediment sorting contrasts: with finer pools and coarser riffles, due to fines being selectively transported off riffle tails on the falling limb of the hydrograph. However, very little tracer material was collected in pool traps at site A, and the pool entrance and trough was always clear of fines at low flow. Pool-troughs have coarser bed material than the adjacent riffles on the Rede (Milan, 2013a). Three possibilities exist that may explain this observation, all of which require further investigation: 1) fines are diverted away from the pool entrance in a similar manner to that found for gravels (see Milan, 2013a); 2) hydraulic forces keep most of the sand in suspension through the pool, preventing it from being deposited on the bed, and flushing material out of the pool. For example MacVicar and Roy (2011) have found that high levels of turbulence intensity resulting from flow deceleration may explain removal of fines from pool heads, in forced pools; 3) during higher flows, most sand is stranded on bar tops and channel margins, in zones of comparatively lower energy at high flow. Sand transport is slower along topographic highs, and therefore material has a tendency to accumulate rather than being dispersed. The opposite can be said for the topographic low points; the thalweg and pools, where sand transport rate is highest for short durations on the rising limb of the hydrograph. Once sand has been flushed through the pools, sediment supply becomes an issue as sand upstream is moving slower over the topographic highs (the riffles), and may become stranded on the bar tops on the falling limb of the hydrograph.

For site B, selective transport (winnowing) of tracer was a feature that occurred during the period (June – November 1996) after seeding during compensation discharges (0.16 m^3s^{-1}). During this 5-month period some sand was transported along the thalweg from the seeded zone, across the right-side of riffle 1 into pool 2 downstream (Fig. 10 A,B). Although hydrograph information is lacking for site B, observations did reveal that flow was elevated between November 1996 and March 1997, with a series of flood peaks related to the overtopping of Catcleugh spillweir, and resulting in sustained elevated flows above the compensation discharge. The exact nature of the hydrographs is unknown. However the tracer deposition in the pools probably occurred on the falling limb of the hydrographs.

5.2 Infiltration

There was no evidence of infiltration into the undisturbed sub-surface framework at site A, possibly due to efficient flushing of fines from the near-surface, but also due to limited void space being available. Some infiltration into the near-surface (0-15 cm) of framework voids was however evident at site B, possibly reflecting less variability in the hydrograph and possible shielding effects of the static armour, that may have prevented fines from being flushed as efficiently. A further possibility is that more void space may have been available at the regulated site (B) in the upper sub-surface gravels, i.e. a thin censored layer, although this could not be quantified from freeze-core samples; the surface *ca*. 5 cm of sediment typically does not freeze very well to the standpipe. Evidence of ingress of the tracer into the sub-surface framework voids of riffle sediments at site B, is supported by Sear (1993; 1995) who found an increase in the percentage of < 2 mm sediments for 79% of the riffles sampled on the river north Tyne, between 1978 and 1988. Petts (1988) has also demonstrated enhanced siltation in two regulated rivers in the UK.

5.3 Downstream movement of tracer wave

Sediment can be routed through river channels either by translation, whereby all features of the sediment wave, including leading and trailing edges, wave apex and center of mass, move downstream (e.g. Meade, 1985), or through dispersion, whereby the wave flattens and spreads out *in situ* and the apex and trailing edge do not migrate downstream (Lisle et al., 2001). Dispersion has been reported as being the most common of these processes in gravel-bed rivers (Lisle et al., 2001). Combined dispersion with translation has also been reported for sand-bed rivers (Cui *et al*., 2003).

For both Rede sites, the tracer clearly showed dispersion rather than translation. Conceptual models of dispersion at the Rede sites are demonstrated in Fig. 14, where the curves show development of the tracer wave, over a sequence of three events. The curves show changes in the χ_t, however this effectively shows how the mass of tracer develops longitudinally through the river channel over time. The mass under the curves should approximately be equal. The position of the centre of mass, the centroid is indicated.

Figure 14 Models of the tracer development to explain centroid movement, A) dispersive wave behaviour shown at site B, and for the first five events at site A. Negative movement of the tracer centroid was shown at site A following events 6, 10 and 11, may possibly be explained by B) re-exposure of buried or infiltrated tracer, or C) preferential erosion of different parts of the tracer wave. Centroid position is indicated by the black, blue and red arrows for a sequence of three events.

The dispersion of the tracer through pool-riffle morphology at each site was clearly non-uniform, and showed a 'lumpy' distribution with χ_t peaks tending to coincide with areas of low shear stress (e.g. bars). Lumpy dispersion of the tracer was a feature also shown by Sear (1996) for the river North Tyne, UK. This factor coupled with the potential vertical interaction of the tracer with both a stable and a mobile gravel-bed, resulted in complex behaviour of the centroid. For all the floods shown at site B and for the first five flows at site A, there was a gradual downstream progression of the tracer following model 1 (Fig. 14A). However, site A showed three negative movements, the first after a discharge peak of 7 m^3s^{-1} (17^{th} Nov 1996), capable of substantial gravel mobilisation (Table 2). The later two negative movements after this date can be disregarded, due to χ_t readings below the detection threshold. Sear (1996) found similar negative movements in his magnetic bedload study on the North Tyne, UK, and explained this through burial and subsequent re-exposure of the buried tracer. However this appears unlikely for the Rede site A, as freeze-core data retrieved in June 1996 did not reveal any burial or infiltration of the tracer. An alternative explanation is demonstrated in model 2 (Fig. 14B,), and is based upon the variable shear stress and non-uniform morphology shown through the study reach (Milan et al., 2001). In this scenario, preferential removal the tracer wave occurs in areas of higher shear stresses, tending to located in areas of lower topography such as pools. In Fig. 14B the majority of tracer is stored in the upstream part of the reach in areas of higher elevation (e.g. a bar). The middle part of the wave has been transported downstream due to higher shear stresses, this sediment gets stored further downstream leading to a double peak distribution. In addition, areas of lower topography experience sediment-transport more frequently than areas of higher topography, hence the tracer could become stranded on higher elevation areas whilst tracer is flushed from lower elevation zones. Complications to the idealised models of sediment wave development involving bar-pool morphology are acknowledged by Lisle (2007) who indicates that topographic forcing by zones of high or low transient transport capacity along the path of the sediment wave can induce differences in deposition and erosion (Beschta, 1983; Nakamura et al., 1995; Church, 1983; Cui and Wilcox, 2005).

6. Conclusion

Artificial magnetic enhancement of iron-stained sands provides a suitable tracer material that mimics saltation-load behaviour in natural fluvial channels. By toasting iron-stained sand in a reducing atmosphere, obtained by mixing flour into the sand, the iron oxide coatings on the silica grains are converted to magnetite and maghaemite. Introduction of tracer material to two gravel-bed reaches, indicated different responses on regulated and unregulated reaches. For the unregulated sinuous reach, most sand was stored on dry bar surfaces and submerged riffle margins. Negligible amounts were found in pools on the unregulated reach (A), suggesting that either 1) fines are diverted away from the pool entrance; 2) hydraulic forces in pools keep fines in suspension and flush all the available sand out of the pool, or 3) sand transport rates are highest along topographic lows leading to well-dispersed sand grains, compared with topographic highs where sand is transported slowly and becomes highly congested. In contrast, fines did appear to be routed through pools in the straight regulated reach (B), although most of the tracer was deposited on riffles overall. In straight reaches all sediment has to be routed through the pool, although may skirt over the shallower parts of the pool cross-section. Hydrograph differences between the regulated at unregulated sites may also play a role in the observed patterns of tracer deposition. Long periods of low compensation flow resulted in selective transport of tracer from the seeded zone at site B across riffle 1, down into pool 2. High flows were experienced after Catcleugh spillweir overtopped in November 1996, resulting in more significant tracer dispersion. Tracer was found in all pools at this site, possibly reflecting longer durations on the falling limb of the hydrographs. However without good quality hydrograph data for site B, it is difficult to examine this in any detail. The hydrograph at site A is very flashy in nature, with a short duration falling limb. As a result the tracer became stranded on topographic highs. In between floods supply limitation of fines to the pools becomes and issue, leaving pools clean of tracer.

None of the tracer appeared to infiltrate into the sub-surface at site A, however small amounts of tracer were detected in the near-surface (0-15 cm) framework voids at site B, possibly reflecting more void space resulting from clear-water flush-out as a consequence of regulated discharges. At the outset of the study, it was anticipated that more infiltration may occur, particularly at site A, where gravel mobilisation was more likely.

Downstream progression of the tracer wave followed a dispersive pattern at both sites. The transport of fine bedload is influenced by variations in shear stress, and morphology, that result in an uneven (lumpy) longitudinal storage of the material. Areas of comparatively higher shear stress along the bed long-profile, for example pools, result in preferential removal of tracer, leading to a perceived negative movement of the centroid. By monitoring the centroid movements and knowing competence duration, V_i was calculated for the study duration, with values of 2.28 m day^{-1} recorded for the unregulated site A, and 0.28 m day^{-1} for regulated site B. These values are greater than those calculated using existing predictive equations developed from gravel tracer data, possibly reflecting differences in the mode of transport between bedload and saltation load.

This study has thrown further insight into the stochastic nature of sediment-transport, yet suggests that fine-sediment tracers have the potential to improve our knowledge of fine-sediment-transport dynamics. The findings of this study also highlight the need for the development of active tracing methodologies for studying the transport of fine-sediments during flood events, to provide an improved picture of sediment routing through pool-riffle morphology.

Acknowledgements

Acknowledgement is made here to Redland Bricks plc and in particular Throckley Brick Works, Newcastle upon Tyne for their cheerful assistance and use of kilns, and Ernie Rice at Lemington glasswork for their help at an earlier stage of the project. The authors would also like to thank Drs. George Heritage, Andy Moores, Clive Waddington, Rachel Suckling, Basil Davis and Mr. Mark Wilde for logistical support in the field. Mr. John Batey of Northumbrian Water is also acknowledged for granting access to site B.

References.

Acornley, R.M., Sear, D.A., 1999. Sediment-transport and siltation of brown trout (*Salmo trutta* L.) spawning gravels in chalk streams. Hydrological Processes 13, 447-458.

Arkell, B., 1985. Magnetic tracing of river bedload. Unpublished PhD thesis. University of Liverpool.

Arkell, B., Leeks, G., Newson, M., Oldfield, F., 1983. Trapping and tracing: some recent observations of supply and transport of coarse sediment from upland Wales. In: Collinson, J.D., Lewin, J. (Eds.) Modern and Ancient Fluvial Systems, Special Publication of the International Association of Sedimentologists 6, pp. 117-129.

Beschta, R. L. 1983. Channel changes following storm-induced hillslope erosion in the Upper Kowai Basin, Torlesse Range, New Zealand. Journal of Hydrology (NZ) 22:93-111.

Beschta, R.L., Jackson, W.L., 1979. The intrusion of fine-sediment into a stable gravel-bed. Journal of the Fisheries Research Board of Canada 36, 204-210.

Brandt, A.A., 2000. Classification of geomorphological effects downstream of dams. Catena 40, 375-401.

Bray, D. I., Church, M., 1980. Armoured versus paved gravel-beds. Journal of the Hydraulics Division of the American Society of Civil Engineering 106, 1937-1940.

Carling, P.A., 1984. Deposition of fine and coarse sand in an open-work gravel-bed, Canadian Journal of Fisheries and Aquatic Sciences 41, 263-270.

Carling, P.A., Orr, H., Kelsey, A., 2006. The dispersion of magnetite bedload tracer across a gravel point-bar and the development of heavy-mineral placers. Ore Geology Reviews 28, 402-416.

Carling, P.A., Reader, N.A., 1982. Structure, Composition and bulk properties of upland stream gravels. Earth Surface Processes and Landforms 7, 349-365.

Church, M. 1983. Pattern of instability in a wandering gravel-bed channel. In: Collinson, J.D., Lewin, J. (Ed.) Modern and Ancient Fluvial Systems. Blackwell Scientific Publications, Oxford, pp169-180.

Church, M.A., Wolcott, J.F., Fletcher, W.K., 1991. A test of equal mobility in fluvial sediment-transport: behaviour of the sand fraction, Water Resources Research 27, 2941-2951.

Crickmore, M. J., 1967. Measurement of sand transport in rivers with special reference to tracer methods. Sedimentology 8, 175-228.

Cui, Y., Parker, G., Pizzuto, J., Lisle, T.E., 2003. Sediment pulses in mountain rivers: 2. Comparison between experiments and numerical predictions. Water Resources Research 39, 1240.

Cui, Y., Wilcox, A.C. 2005. Numerical modeling of sediment-transport upon dam removal: Application to Marmot Dam in Sandy River, Oregon. In: Garcia, M. H. (Ed.) Reston, VA.

de Almeida, G. A. M., Rodriguez, J. F., 2012. Spontaneous formation and degradadtion of pool-riffle morphology and sediment sorting using a simple fractional transport model. Geophysical Research Letters 39, L06407, DOI:10.1029/2012GL051059

Einstein, H.A., 1968. Deposition of suspended particles in a gravel-bed. Journal of the Hydraulics Division ASCE 94, 1197-1205.

Fassnacht, H., McClure, E.M., Grant, G.E., Klingeman, P.C., 2003. Downstream effects of the Pelton-Round Butte hydroelectric project on bed load transport, channel morphology, and channel-bed texture, lower Deschutes River, Oregon. Water Science and Application 7, 175–207.

Ferguson, R.I., Wathen, S.J., 1998. Tracer-pebble movement along a concave river profile: Virtual velocity in relation to grain-size and shear stress. Water Resources Research 34, 2031-2038.

Frostick, L.E. Lucas, P.M., Reid, I., 1984. The infiltration of fine matrices into coarse-grained alluvial sediments and its implications for stratigraphic interpretation. Journal of the Geological Society of London 141, 955-965.

Fuller, I.C., Large, A.R.G., Milan, D.J., 2003. Quantifying channel development and sediment transfer following chute cut-off in a wandering gravel-bed river. Geomorphology, 54, 307-323.

Galay, V.J. Causes of river bed degradation. Water Resources Research 19, 1057-1090.

Garde, R.J., Ranga Raju, K.G., 1977. Mechanics of sediment-transportation and alluvial stream problems, Wiley Eastern Ltd, 483pp.

Haschenburger, J.K. Church, M., 1998. Bed material transport estimated from the virtual velocity of sediment. Earth Surface Processes and Landforms 23, 791-808.

Haschenburger, J.K., 2011. The rate of fluvial gravel dispersion. Geophysical Research Letters 38, L24403.

Heritage GL, Milan DJ, Large ARG, Fuller I., 2009**.** Influence of survey strategy and interpolation model upon DEM quality. Geomorphology 112, 334-344.

Hubbell, D.W., Sayre, W.W., 1964. Sand transport studies with radioactive tracers. Journal of the Hydraulics Division of the American Society of Civil Engineers 91(HY5), 139-148.

Hughes, N., 1992. Heavy mineral distribution in upland gravel-bed rivers. Unpublished PhD Thesis, Department of Geography, Loughborough University.

Jackson WL, Beschta RL., 1982. A model of two-phase bedload transport in an Oregon Coast Range stream. Earth Surface Processes and Landforms 7, 517-527.

Jones, J.I., Murphy, J.F., Collins, A.L., Sear, D.A., Naden, P.S., Armitage, P.D., 2011. The impact of fine-sediment on macro-invertebrates. River Research and Applications 27(1), doi:10.1002/raa.1516

Keller, E.A., 1971. Areal sorting of bed-load material: the hypothesis of velocity reversal. Geological Society of America Bulletin 82, 753-756.

Kondolf, G.M., Williams, J.G., Horner, T.C. Milan, D.J., 2008. Quantifying physical degradation of spawning habitat. In: Sear, D.A., DeVries, P., Greig, S. (Eds.). Salmon spawning habitat in rivers: Physical controls, biological responses and approaches to remediation. American Fisheries Society Symposium 65, 249-274.

Lisle, T.E. and Hilton, S., 1999. Fine bed material in pools of natural gravel-bed channels, Water Resources Research 35, 1291-1304.

Lisle, T.E., 1979. A sorting mechanism for riffle-pool sequence. Geological Society of America Bulletin 90, 1142-1157

Lisle, T.E., 1989. Sediment-transport and resulting deposition in spawning gravels, North Coastal California. Water Resources Research 25(6), 1303-1319.

Lisle, T.E., 2007. The evolution of sediment waves influenced by varying transport capacity in heterogeneous rivers. In: In Habersack, H., Piegay, H, Rinaldi, M. (Eds.) Gravel-bed Rivers VI: From Process understanding to river restoration, Developments in Earth Surface Processes 11, pp 443-469.

Lisle, T.E., Cui, Y., Parker, G. Pizzuto, J.E., Dodd, A.M. 2001. The dominance of dispersion in the evolution of bed material waves in gravel-bed rivers. Earth Surface Processes & Landforms 26, 1409-1422.

Lisle, T.E., Hilton, S., 1992. The volume of fine-sediment in pools: an index of sediment supply in gravel-bed streams. Water Resources Bulletin 28(2), 371-383.

MacVicar BJ, Roy AG., 2011. Sediment mobility in a forced riffle-pool. Geomorphology 125, 445-456.

Meade, R.H., Parker, R.S., 1985. Sediment in rivers of the United States. U.S. Geological Survey Water-Supply Paper 2275, Washington, DC.

Milan, D.J., 1996. The application of freeze-coring for siltation assessment in a recently regulated stream. In: Merot, P., Jigorel, A. (Eds.) Hydrologie dans les pays celtiques. Actes du 1er Colloque interceltique d'Hydrologie et de Gestion des Eaux. Organise par CEMAGREF, DIREN, IFREMER, INRA, INSA. Rennes France, 8-11 Juillet 1996, Les Colloques no 79, pp253-266.

Milan, D.J., 2000. Sand and gravel transport through a riffle-pool sequence. Unpublished PhD thesis, Department of Geography, University of Newcastle upon Tyne, 341pp.

Milan, D.J., 2013a. Sediment routing hypothesis for pool-riffle maintenance. Earth Surface Processes and Landforms. DOI: 10.1002/esp.3395

Milan, D.J., 2013b. Virtual velocity of tracers in a gravel-bed river using size-based competence duration. Geomorphology, http://dx.doi.org/10.1016/j.geomorph.2013.05.018

Milan, D.J., Heritage, G.L., Large, A.R.G., 2002. Tracer pebble entrainment and deposition loci: influence of flow character and implications for riffle-pool maintenance. In: Jones, S.J., Frostick, L.E. (Eds.) Sediment flux to basins: causes, controls and consequences, Geological Society of London Special Publications 191, 133-148.

Milan, D.J., Heritage, G.L., Large, A.R.G., Charlton, M.E., 2001. Stage-dependent variability in shear stress distribution through a riffle-pool sequences. Catena 44, 85-109.

Milan, D.J., Petts, G.E. and Sambrook, H., 2000. Regional variations in sediment structure of trout streams in southern England. Aquatic Conservation 10, 407-420

Mosely, M.P., 1978. Bed material transport in the Tamaki River near Dannevirke, North Island, New Zealand. New Zealand Journal of Science 21, 619-626.

Nakamura, F., H. Maita, Araya, T. 1995. Sediment routing analysis based on chronological changes in hillslope and riverbed morphologies. Earth Surface Processes and Landforms 20, 333-346.

Oldfield, F., Thompson, R., Dicson, D.P.E., 1981. Artificial enhancement of stream bedload: a hydrological application of supermagnetism. Physics of the Earth and Planetary Interiors 26, 107-124.

Parker, R. T. G., Dhamotheran, P.C. Stefan, H., 1982. Model experiments on mobile, paved gravel-bed streams. Proceedings of the American Society of Civil Engineers, Journal of the Hydraulics Division 107, 1395-1408.

Petts, G. E., Thoms, M. C., Brittan, K., Atkin, B., 1989. A freeze-coring technique applied to pollution by fine-grained sediments in gravel-bed rivers, The Science of the Total Environment 84, 259-272.

Petts, G.E., 1979. Complex response of river channel morphology subsequent to reservoir construction. Progress in Physical Geography 3, 329-362.

Petts, G.E., 1984. Impounded Rivers, Wiley, Chichester.

Petts, G.E., 1988. Accumulation of fine-sediment within substrate gravels along two regulated rivers, UK. Regulated Rivers: Research and Management 2, 141-154.

Petts, G.E., Gurnell, A.M., 2005. Dams and geomorphology: research progress and future directions. Geomorphology 71, 27-47.

Powell, D.M., 1998. Patterns and processes of sediment sorting in gravel-bed rivers. Progress in Physical Geography 22, 1-32.

Rathburn, R.E., Kennedy, V.C., 1978. Transport and dispersion of flourescent tracer particles for the dune-bed condition, Atrisco Feeder Canal near Bernalillo, New Mexico. US Geological Survey Professional Paper 1037.

Reid, I., Frostick, L.E., Layman, J.T., 1985. The incidence and nature of bedload transport during flood flows in coarse-grained alluvial channels. Earth Surface Processes and Landforms 10, 33-44.

Richards, K.S., Clifford, N., 1991. Fluvial geomorphology: structured beds in gravelly rivers. Progress in Physical Geography 15, 407-422.

Rummery, T.A., Oldfield, F., Thompson, R., Newson, M., 1979. Magnetic tracing of stream bedload. Geophysical Journal of the Royal Astrological Society 57, 278-279.

Schälchli, U., 1995. Basic equations for siltation of riverbeds. Journal of Hydraulic Engineering 121(3), 274-287.

Sear, D. A., 1992. Sediment-transport processes in riffle-pool sequences and the effects of river regulation for hydroelectric power in the River North Tyne, Unpublished PhD thesis, University of Newcastle upon Tyne.

Sear, D. A., 1995. Morphological and sedimentological changes in a gravel-bed river following 12 years of flow regulation for hydropower. Regulated Rivers: Research and Management 10, 247-264.

Sear, D.A., 1993. Fine-sediment infiltration into gravel spawning beds within a regulated river experiencing floods: ecological implications for salmonids. Regulated Rivers Research and Management 8, 373-390.

Sear, D.A., 1996. Sediment-transport processes in pool-riffle sequences. Earth Surface Processes and Landforms 21, 241-262.

Stephenson, A., de Sa 1970. A simple method for the measurement of the temperature variation of initial magnetic susceptibility between 77 and 1000 K. Journal of Physics E: Scientific Instruments 3 59-61.

Sutherland, A.J., 1987. Static armour layers by selective erosion. In: Thorne, C.R., Bathurst, J.C., Hey, R.D. (Eds.) Gravel-bed rivers, John Wiley and Sons, Chichester, UK, pp243-268.

van der Post, K.D., Oldfield, F. and Voulgaris, G. 1994. Magnetic tracing of beach sand: preliminary results, Proceedings Coastal Dynamics '94, approved for publication by the Waterway, Port, Coastal and Ocean Division/ASCE, February 21-25, 1994, Barcelona, Spain.

Vericat, D., Batalla, R.J., 2005. Sediment-transport in a highly regulated fluvial system during two consecutive floods (Lower Ebro River, NE Spain). Earth Surface Processes and Landforms 30, 385–402.

Vetter, T., 2011. Riffle-pool morphometry and stage-dependant morphodybamics of a large floddplain river (Vereinigte Mulde, Sachsen-Anhalt, Germany). Earth Surface Processes and Landforms 36, 1647-1657.

Williams, G.P., Wolman, M.G., 1984. Downstream effects of dams on alluvial rivers. US Geological Survey Professional Paper 1986, Washington, DCWolman, M.G., 1954. A method of sampling coarse river gravels, Transactions of the American Geophysical Union 35, 951-956.

Wyżga, B., 1993. River response to channel regulation: case study of the Raba river, Carpathians, Poland. Earth Surface Processes and Landforms, 18, 541-556.

Table and Figure Captions

Table 1 Mean and range of χ_t values, and interpolation error for the contour plots (Figs. 9 and 10), recorded at each site over the study period

Table 2 A flood-by-flood account of the tracer position though the Rede riffle-pool sequence for Site A

Table 3 A flood-by-flood account of the tracer position though the Rede riffle-pool sequence for Site B

Figure 1 Study location A) Rede catchment, B) site A, C) site B. Magnetically enhanced sand was seeded at the upstream end of each reach, as indicated by the grey boxes. The approximate extent of pools (P), riffles (R), and bars (B) are highlighted. Flow direction is indicated by the arrow. Position of basket and grab samples are highlighted as red points.

Figure 2 Discharge hydrograph over the study duration recorded at site A. Green arrow indicates date of tracer seeding, red arrows indicate sediment sampling dates.

Figure 3 Results of laboratory trials into the optimum conditions for magnetic enhancement, A) Comparison of enhanced tracer sands and background samples taken from the Rede site, B) effect of temperature, C) influence of heating duration at 700°C, D) influence of reducing agent concentration

Figure 4 Sand tracing experiment, A) Magnetic enhancement of iron stained sand: sand-flour mixture was placed in large tins and roasted in the 'specials kiln' at Redland Brick Works, Newcastle upon Tyne, B) introduction of magnetic sand to the channel at site B, C) raking sand over the bed surface at site A, D) back coloured magnetic sand on the pool bed at site B shortly after introduction, E) deposition on the edge and surface of point bar 3 at site A, F) close up of surface deposition on the edge of bar 3 at site A.

Figure 5 Fine-sediment sampling, A) Basket trapping, B) Freeze-coring

Figure 6 Background χ_t distribution for matrix sediments sampled at sites A and B.

Figure 7 Cumulative grain-size information for the river Rede, A) Armour and framework grain-size distribution for sites A and B, B) void, matrix, unenhanced and magnetically enhanced sand grain-size distributions.

Figure 8 Relationship between mean sediment accumulation (based upon 31 traps at each site) and discharge for a) site A, and b) site B. Closed symbols represent periods where magnetic tracer was detectable within the system.

Figure 9 Spatial patterns of magnetic susceptibility of fine-sediments deposited over pool-riffle morphology at site A, A) Background characteristics, B) magnetic susceptibility on 30th April 1996, one week after tracer emplacement following a peak discharge of 0.5 m^3s^{-1}, and C) magnetic susceptibility on 22nd May 1996, following a 3.6 m^3s^{-1} event.

Figure 10 Spatial patterns of magnetic susceptibility of fine-sediments deposited over pool-riffle morphology at site B, A) Characteristics immediately following tracer emplacement on 13th June 1996, indicating background conditions, magnetic susceptibility on B) 2nd Nov 1996 following a steady discharge of 0.16 m^3s^{-1}, C) 12th Nov 1996, following a peak flow of 11.0 m^3s^{-1}, D) 23rd Dec 1996,, following a peak discharge of11.9 m^3s^{-1}, E) 11th March 1997, following a peak discharge of 14.4 m^3s^{-1}.

Figure 11 Downstream magnetic susceptibility waveform following different flow events for site A.

Figure 12 Downstream magnetic susceptibility waveform following different flow events for site B.

Figure 13 Vertical distribution in magnetic susceptibility of < 2 mm samples taken from freeze-cores, A) background values before introduction of the tracer at site A, B) values after the first flow responsible for movement of the tracer 3.2 m^3s^{-1}, sampled in June 1996 at site A, C) background values before introduction of the tracer at site B, D) values after a series of high winter flows peaking at 14.4 m^3s^{-1}, sampled in March 1997 at site B. Levels of detection are indicated by the dashed red lines.

Figure 14 Models of tracer development to explain centroid movement, A) dispersive wave behaviour shown at site B, and for the first five events at site A. Negative movement of the tracer centroid was shown at site A following events 6, 10 and 11, may possibly be explained by B) re-exposure of buried or infiltrated tracer, or C) preferential erosion of different parts of the tracer wave. Centroid position is indicated by the black, blue and red arrows for a sequence of three events.

Table 1 Mean and range of χ_t values, and interpolation error for the contour plots (Figs. 9 and 10), recorded at each site over the study period

	Date	Mean χ_t and range in brackets	Mean error and range in brackets (χ_t)
Site A	14.04.96	6.67 (1.05 to 21.48)	0.00 (-0.33 to 0.39)
	30.04.96	18.18 (0.10 to 93.30)	0.01 (-2.42 to 2.29)
	22.05.96	14.70 (0.40 to 130.70)	0.01 (-4.64 to 5.40)
Site B	13.06.96	13.36 (3.04 to 64.28)	-1.59 (-31.07 to 13.61)
	02.11.96	7.99 (4.98 to 50.00)	-0.28 (-6.17 to 5.29)
	12.11.96	20.07 (1.99 to 79.43)	1.81 (-11.15 to 51.86)
	23.12.96	34.63 (2.10 to 61.91)	0.98 (-10.10 to 15.28)
	11.03.97	30.64 (2.22 to 63.08)	0.32 (-14.97 to 13.37)

Table 2 A flood-by-flood account of tracer position though the Rede riffle-pool sequence for Site A

Event sequence	Date	Centroid position downstream of emplacement site (m)	Movement L (m)	Previous peak Q (m^3s^{-1})
1	22.5.96	84.8	84.8	3.2
2	6.6.96	96.3	11.5	0.54
3	10.9.96	101.8	5.5	2.08
4	14.10.96	111.1	9.3	3.39
5	2.11.96	152.2	41.1	5.44
6	17.11.96	146.2	-6.0	7.12
7	10.12.96	149.8	3.6	4.13
8	22.12.96	178.5	28.7	4.09
9	15.1.97	199.2	20.7	1.23
10	31.1.97	178.9	-20.3	3.81
11	8.2.97	155.1	-23.9	3.99
12	11.3.97	201.4	46.3	8.62

Table 3 A flood-by-flood account of tracer position though the Rede riffle-pool sequence for Site B

Event sequence	**Date**	**Centroid position downstream of emplacement site (m)**	**Movement *L* (m)**	**Previous peak Q (m^3s^{-1})**
1	25.9.96	23.7	23.7	0.16
2	2.11.96	38.2	14.5	0.16
3	12.11.96	51.0	12.8	11.0
4	23.12.96	53.5	2.5	11.9
5	20.1.97	62.5	9.0	6.4
6	11.3.97	76.1	13.6	14.4

Fig 1

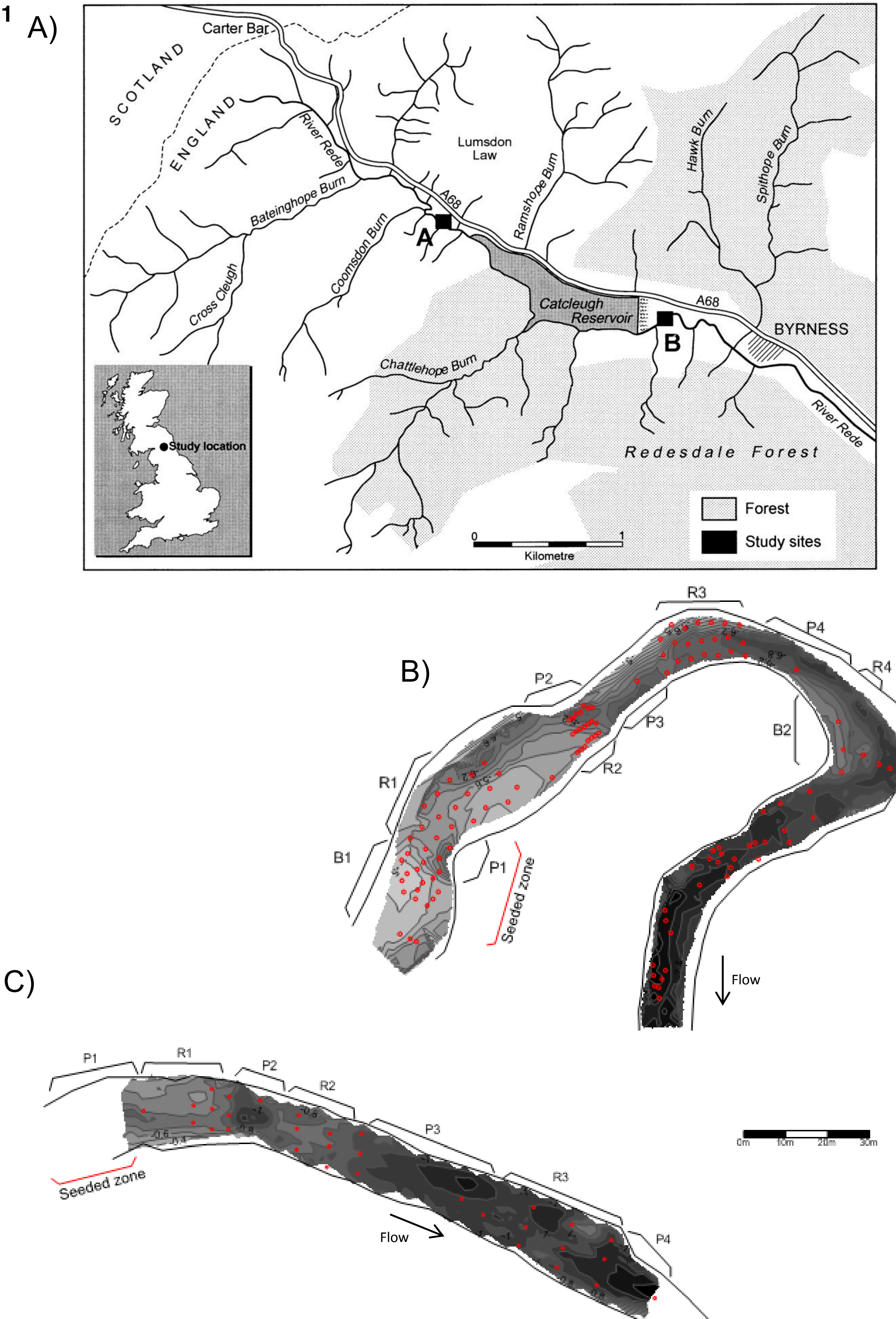

A)
Carter Bar
SCOTLAND
ENGLAND
River Rede
Bateinghope Burn
Cross Cleugh
Coomsdon Burn
A68
A
Lumsdon
Law
Ramshope Burn
Hawk Burn
Spithope Burn
Catcleugh
Reservoir
B
BYRNESS
Chattlehope Burn
River Rede
Redesdale Forest
Study location
Forest
Study sites
0
1
Kilometre
B)
R1
B1
P1
Seeded zone
P2
R2
P3
R3
P4
R4
B2
P5
Flow
C)
P1
R1
P2
R2
P3
R3
P4
Seeded zone
Flow
0m
10m
20m
30m

Fig 2

Fig 2

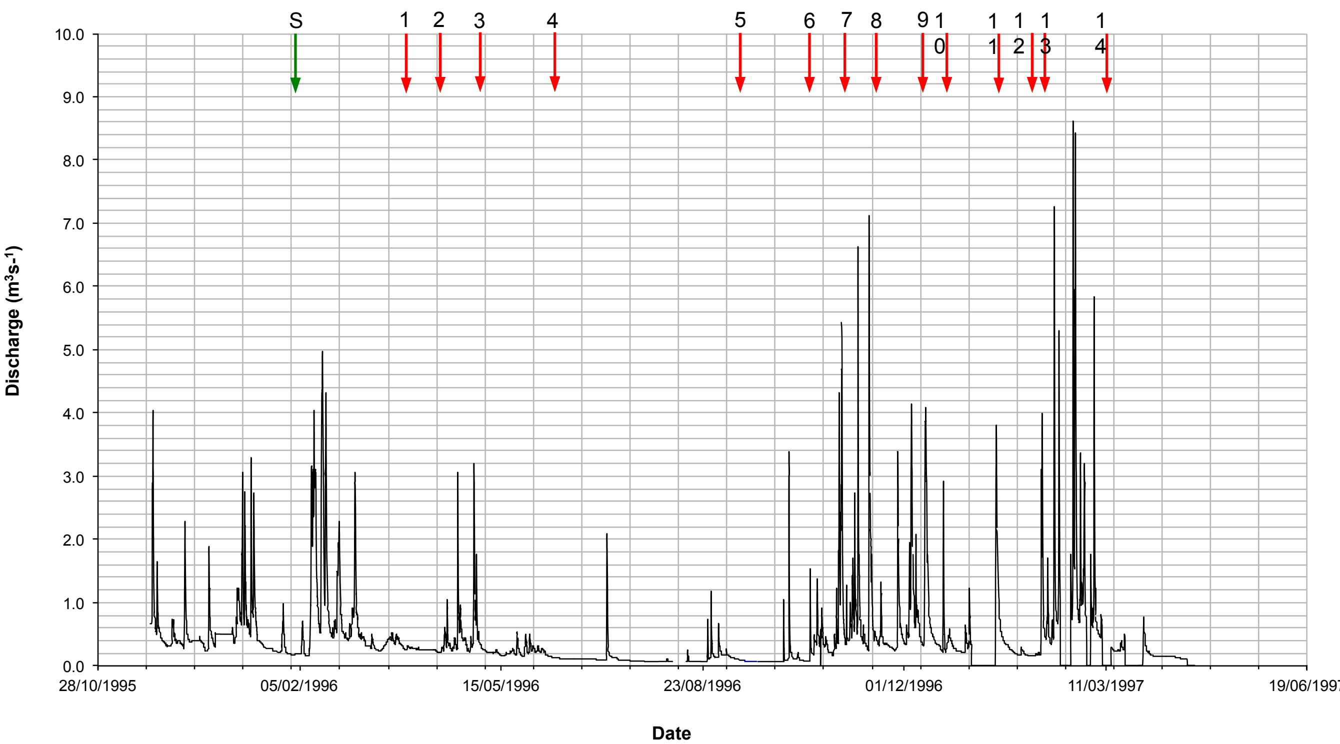
S
1
2
3
4
5
6
7
8
9
10
11
12
13
14
10.0
9.0
8.0
7.0
6.0
5.0
4.0
3.0
2.0
1.0
0.0
Discharge (m³s⁻¹)
28/10/1995
05/02/1996
15/05/1996
23/08/1996
01/12/1996
11/03/1997
19/06/1997
Date

Fig 3

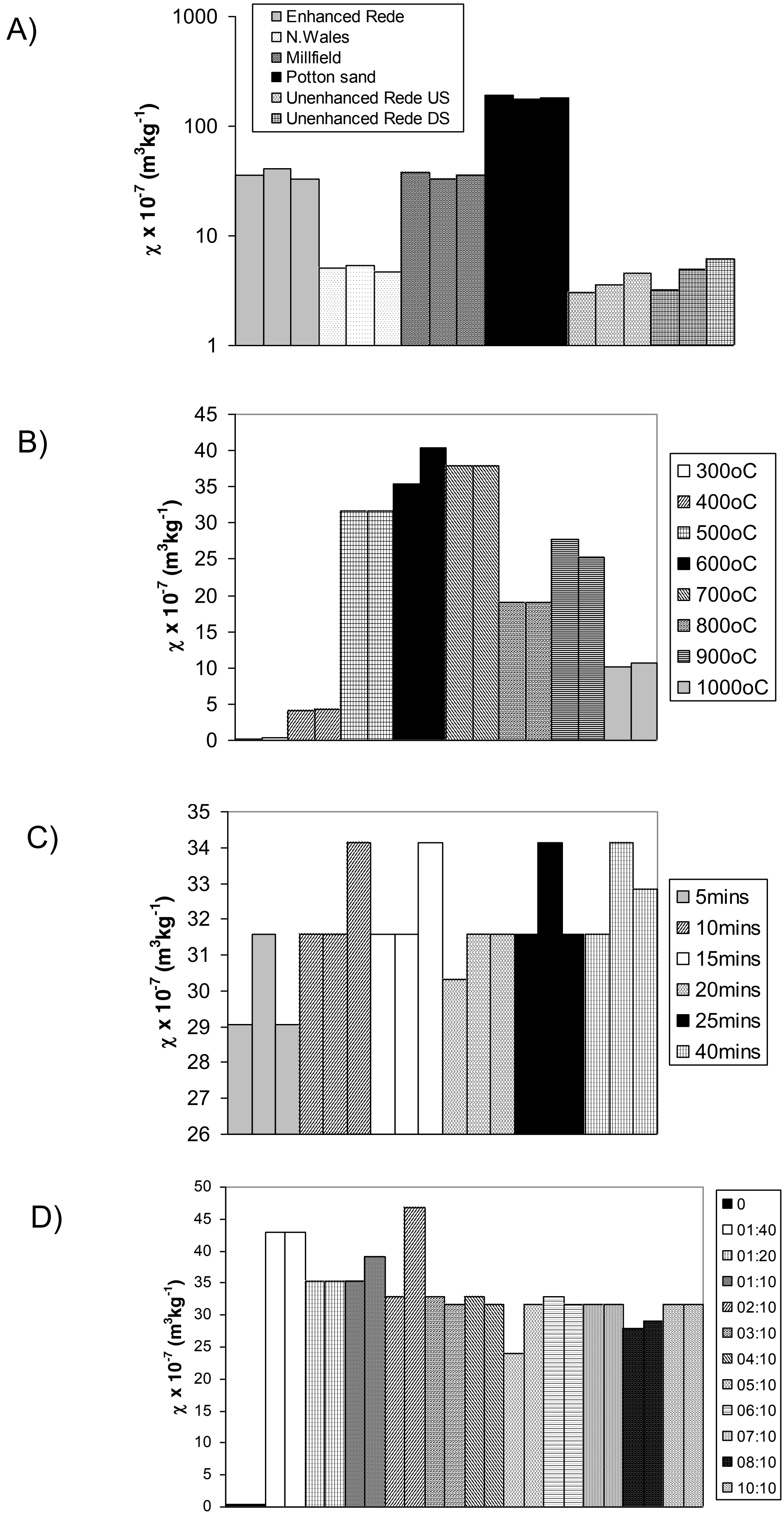
A)
1000
100
10
1
χ x 10-7 (m3kg-1)
Enhanced Rede
N.Wales
Millfield
Potton sand
Unenhanced Rede US
Unenhanced Rede DS
B)
45
40
35
30
25
20
15
10
5
0
χ x 10-7 (m3kg-1)
300oC
400oC
500oC
600oC
700oC
800oC
900oC
1000oC
C)
35
34
33
32
31
30
29
28
27
26
χ x 10-7 (m3kg-1)
5mins
10mins
15mins
20mins
25mins
40mins
D)
50
45
40
35
30
25
20
15
10
5
0
χ x 10-7 (m3kg-1)
0
01:40
01:20
01:10
02:10
03:10
04:10
05:10
06:10
07:10
08:10
10:10

Fig 4

Click here to download high resolution image

Fig 4

Fig 5

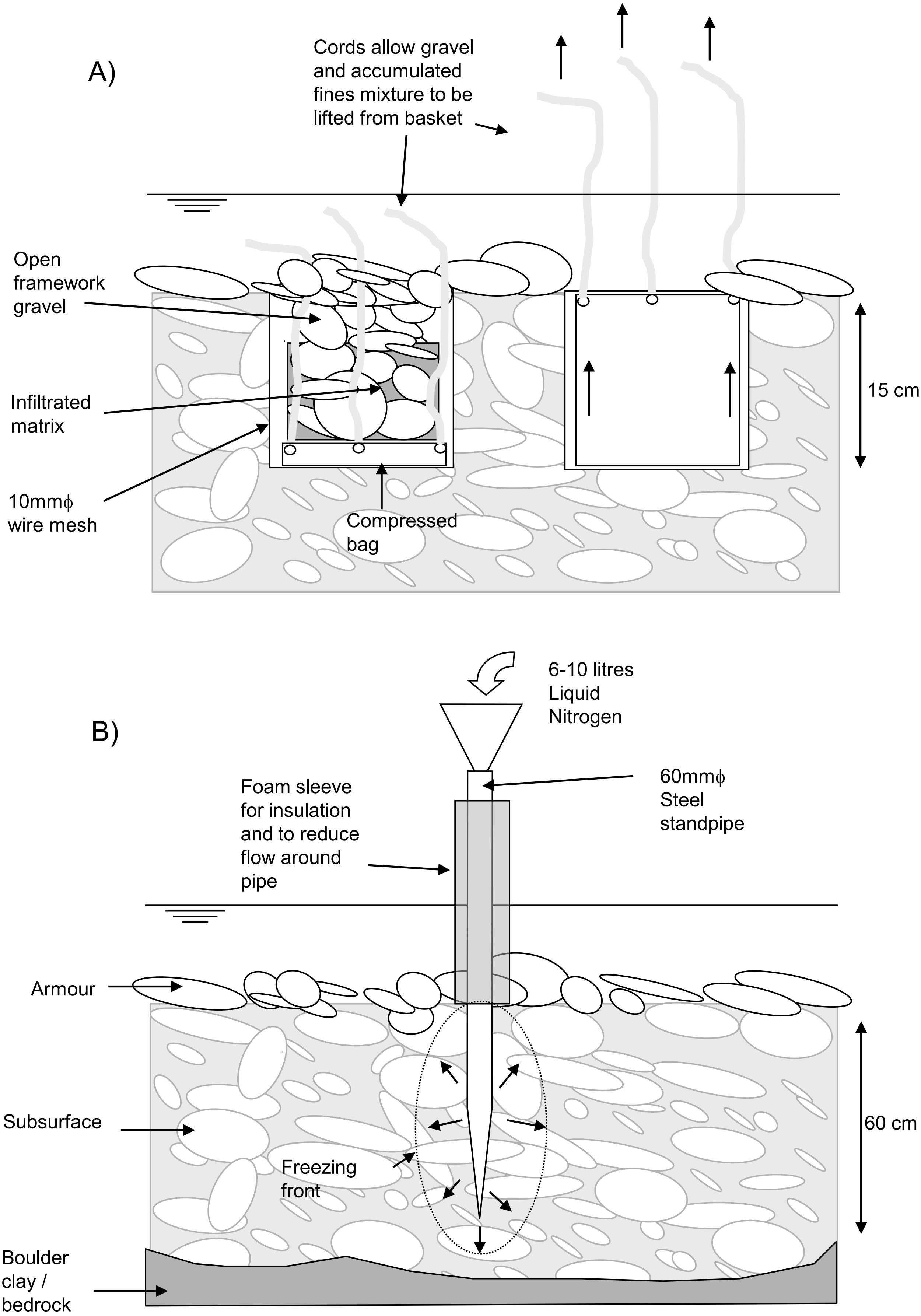
A)
Cords allow gravel
and accumulated
fines mixture to be
lifted from basket
Open
framework
gravel
Infiltrated
matrix
10mmϕ
wire mesh
Compressed
bag
15 cm
B)
6-10 litres
Liquid
Nitrogen
Foam sleeve
for insulation
and to reduce
flow around
pipe
60mmϕ
Steel
standpipe
Armour
Subsurface
Freezing
front
60 cm
Boulder
clay /
bedrock

Fig 6

Fig 6

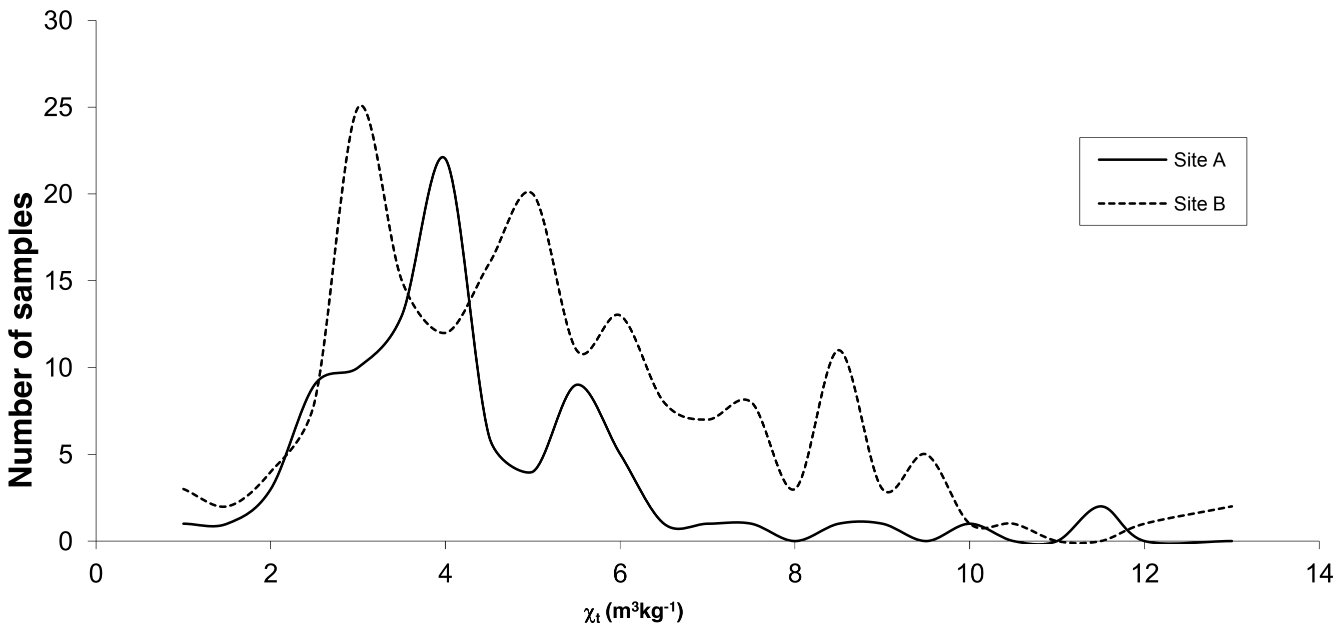

30
25
20
15
10
5
0
Number of samples
0
2
4
6
8
10
12
14
χ_t (m^3kg^{-1})
Site A
Site B

Fig 7

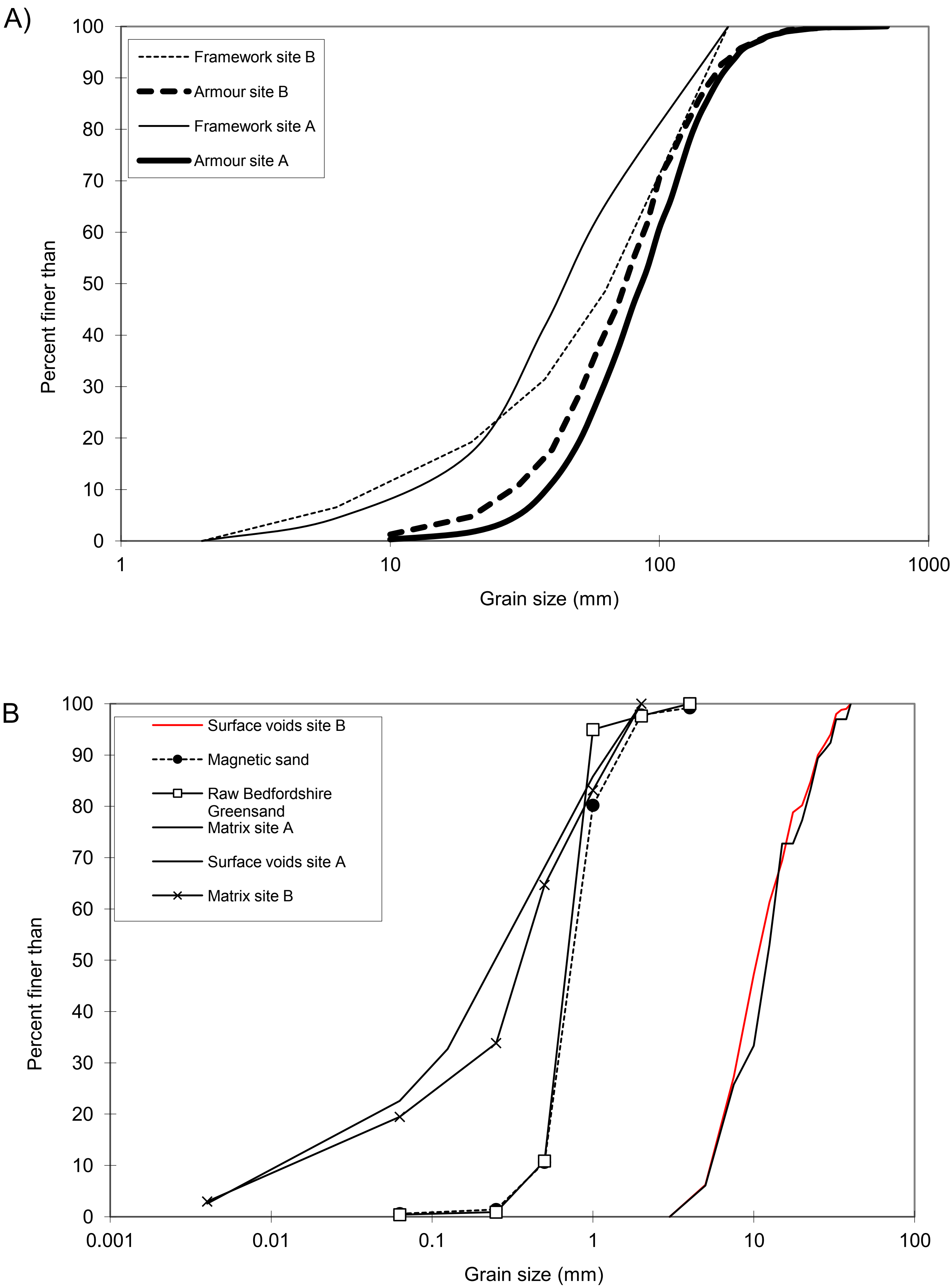
A)
Framework site B
Armour site B
Framework site A
Armour site A
Percent finer than
Grain size (mm)
B
Surface voids site B
Magnetic sand
Raw Bedfordshire Greensand
Matrix site A
Surface voids site A
Matrix site B
Percent finer than
Grain size (mm)

Fig 8
Fig 8

A)

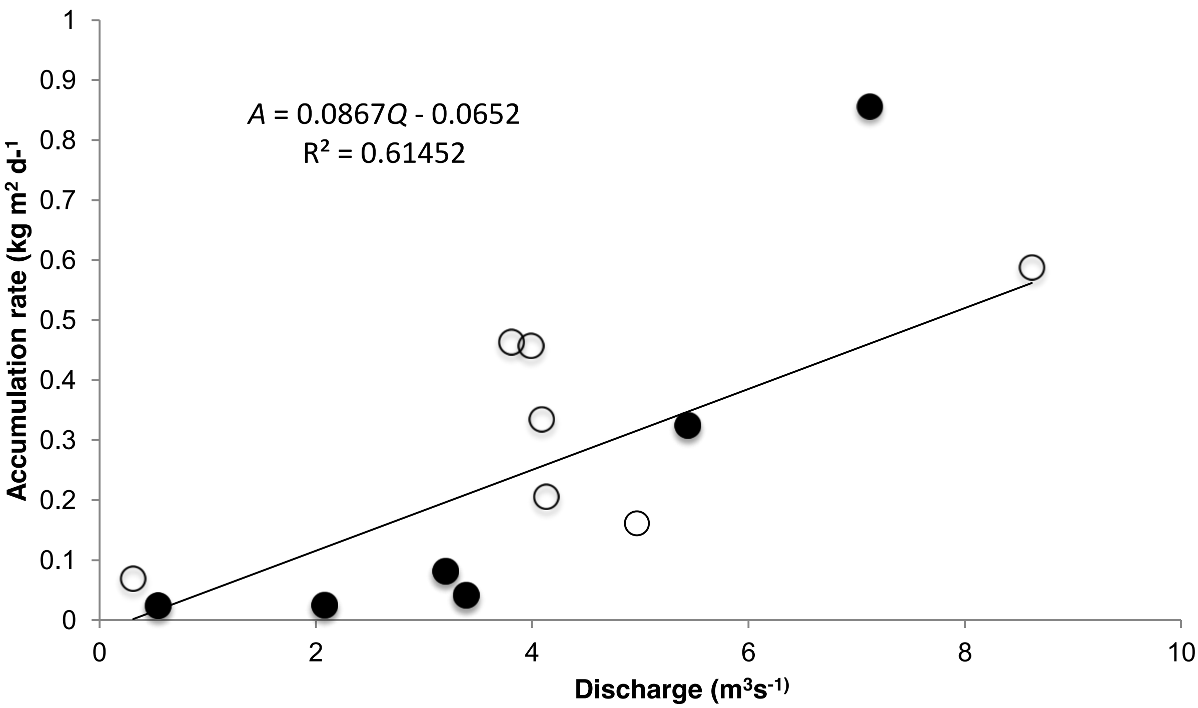

$A = 0.0867Q - 0.0652$
$R^2 = 0.61452$
Accumulation rate (kg m² d⁻¹
Discharge (m³s⁻¹)
0
0.1
0.2
0.3
0.4
0.5
0.6
0.7
0.8
0.9
1
0
2
4
6
8
10

B)

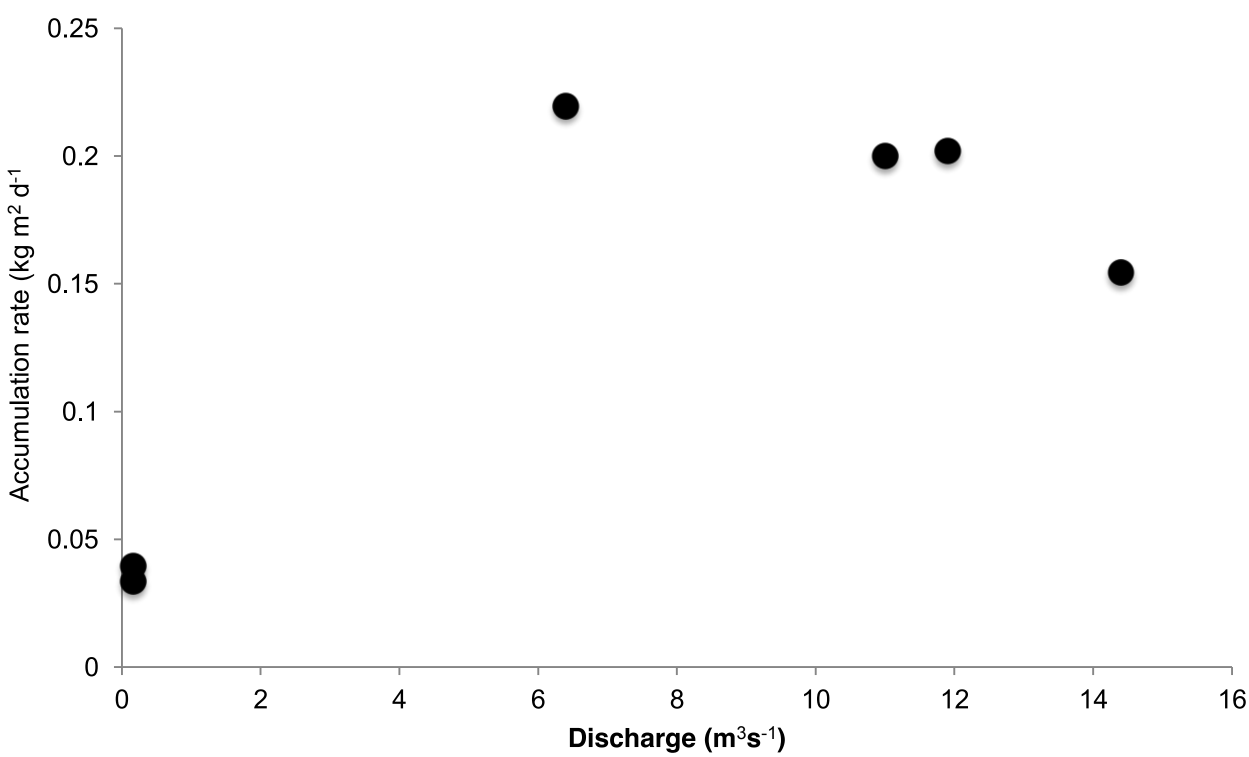

Accumulation rate (kg m² d⁻¹
Discharge (m³s⁻¹)
0
0.05
0.1
0.15
0.2
0.25
0
2
4
6
8
10
12
14
16

Fig 9

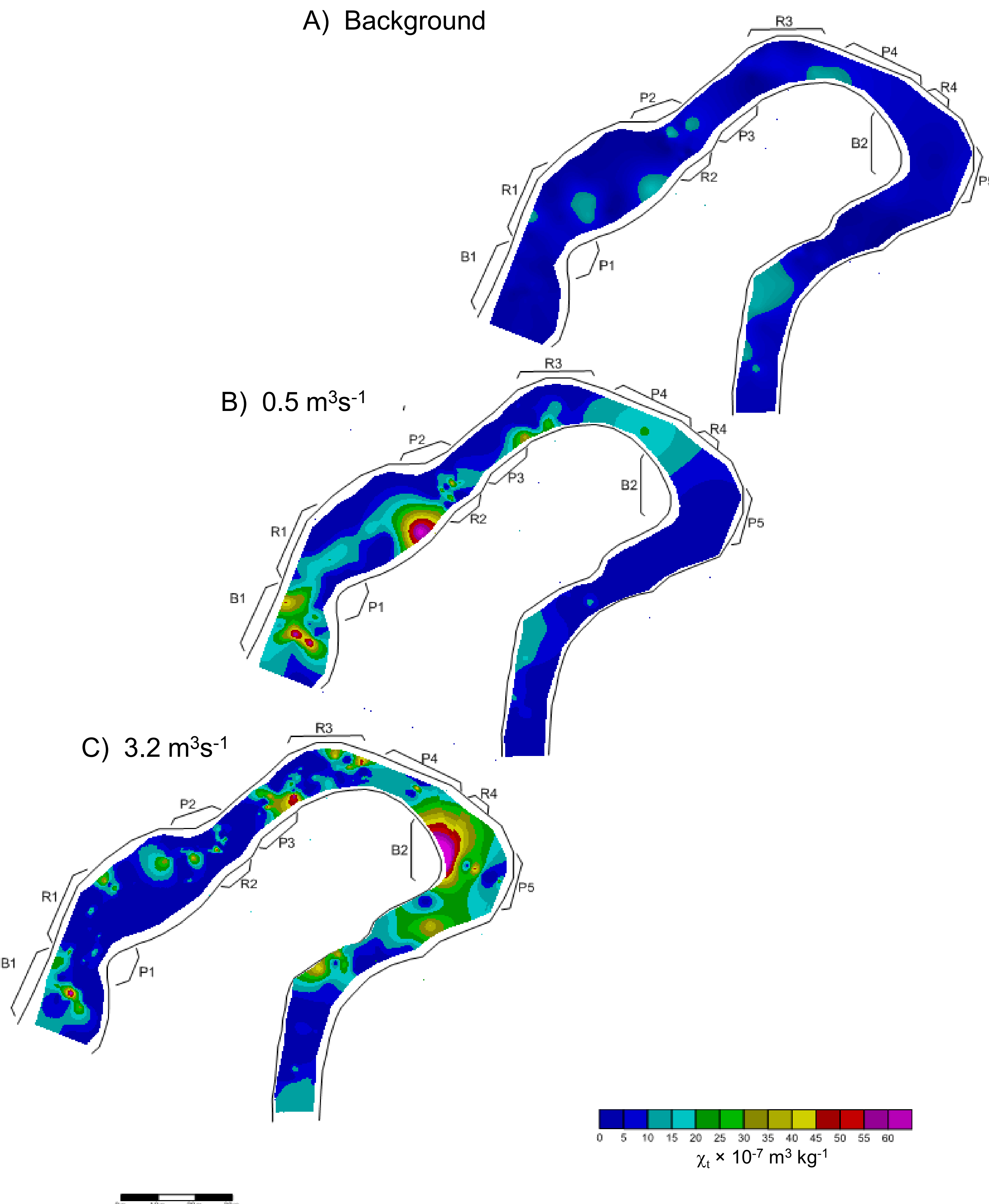
A) Background
B) 0.5 m3s-1
C) 3.2 m3s-1
R1
R2
R3
R4
P1
P2
P3
P4
P5
B1
B2
0
5
10
15
20
25
30
35
40
45
50
55
60
χt × 10-7 m3 kg-1
0m
10m
20m
30m

Fig 10

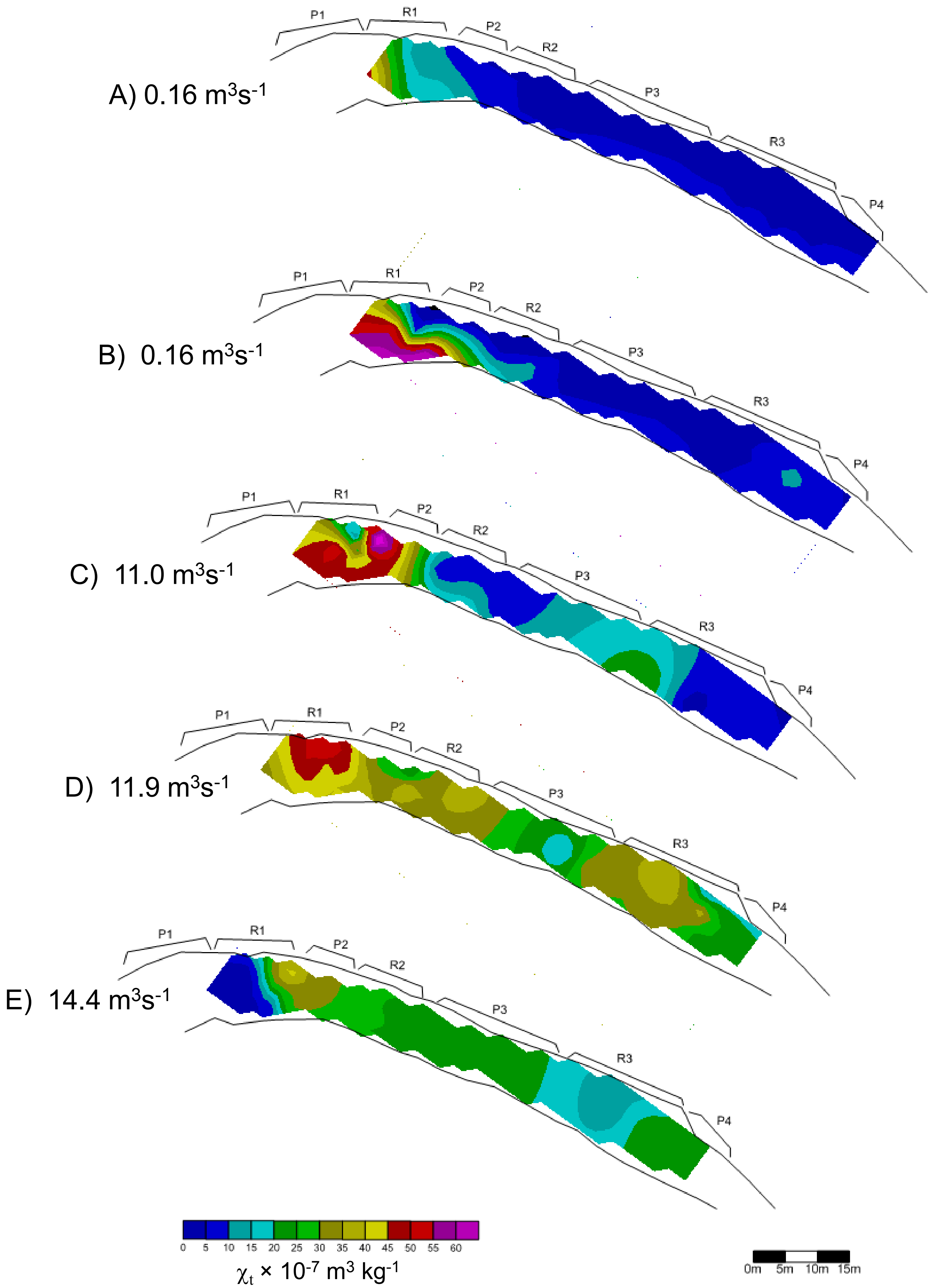
A) 0.16 m³s⁻¹
B) 0.16 m³s⁻¹
C) 11.0 m³s⁻¹
D) 11.9 m³s⁻¹
E) 14.4 m³s⁻¹
P1
R1
P2
R2
P3
R3
P4
0 5 10 15 20 25 30 35 40 45 50 55 60
χt × 10⁻⁷ m³ kg⁻¹
0m 5m 10m 15m

Fig 11

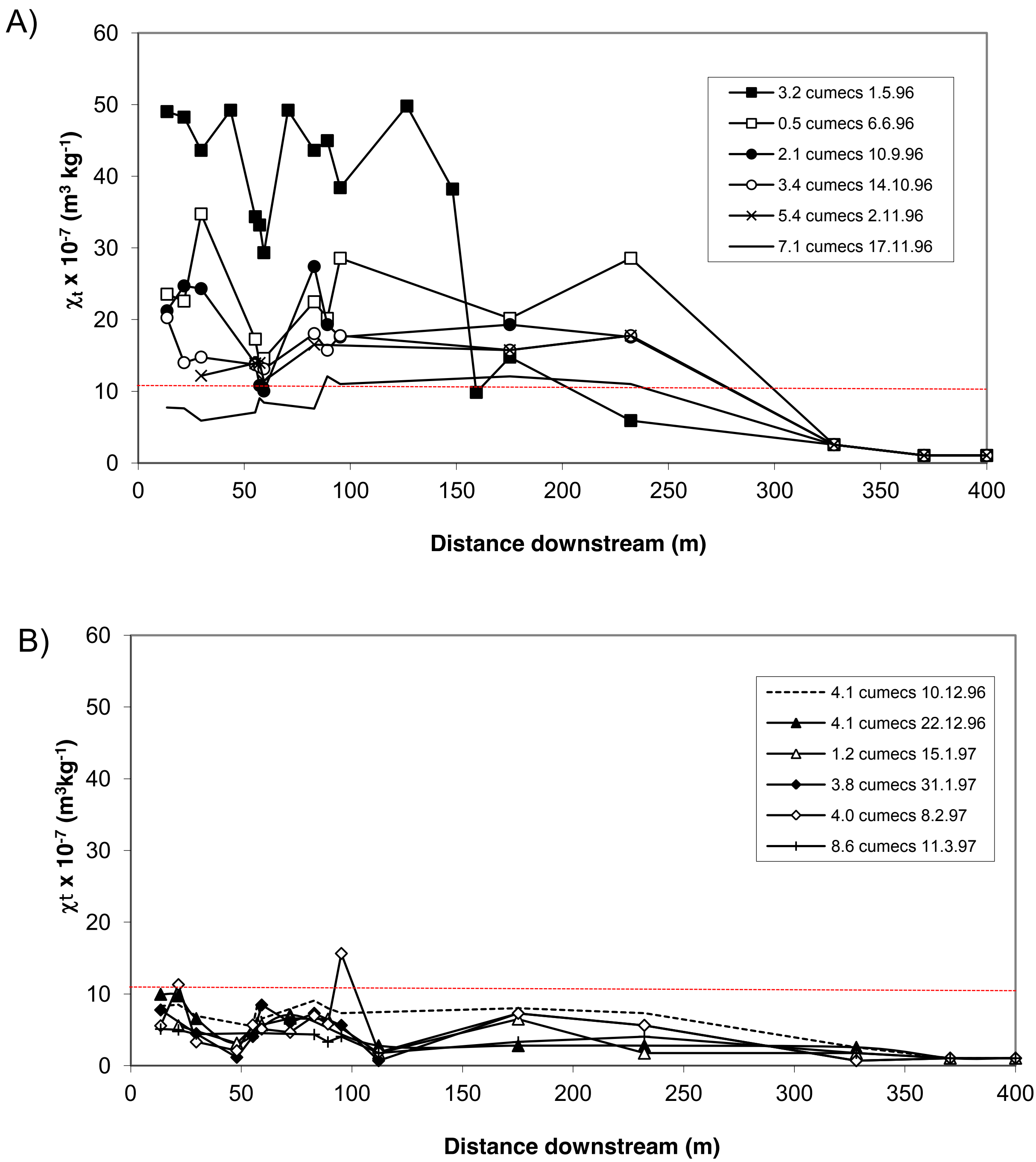

A)
χ_t x 10^{-7} (m^3 kg^{-1})
Distance downstream (m)
3.2 cumecs 1.5.96
0.5 cumecs 6.6.96
2.1 cumecs 10.9.96
3.4 cumecs 14.10.96
5.4 cumecs 2.11.96
7.1 cumecs 17.11.96
B)
χt x 10^{-7} (m^{3}kg^{-1})
Distance downstream (m)
4.1 cumecs 10.12.96
4.1 cumecs 22.12.96
1.2 cumecs 15.1.97
3.8 cumecs 31.1.97
4.0 cumecs 8.2.97
8.6 cumecs 11.3.97

Fig 12

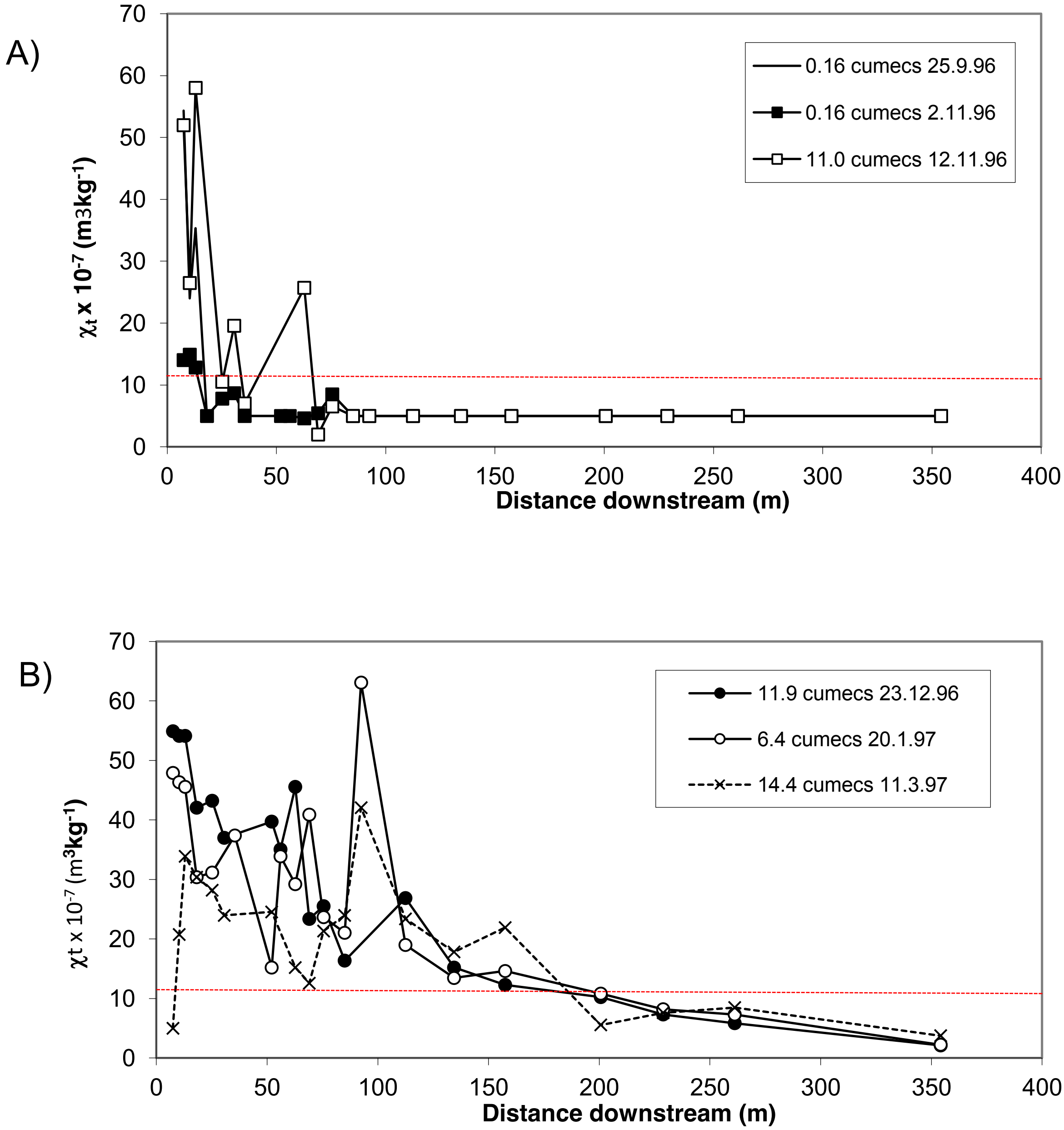
A)
0.16 cumecs 25.9.96
0.16 cumecs 2.11.96
11.0 cumecs 12.11.96
χt x 10-7 (m3kg-1)
Distance downstream (m)
B)
11.9 cumecs 23.12.96
6.4 cumecs 20.1.97
14.4 cumecs 11.3.97
χt x 10-7 (m3kg-1)
Distance downstream (m)

Fig 13
Fig 13

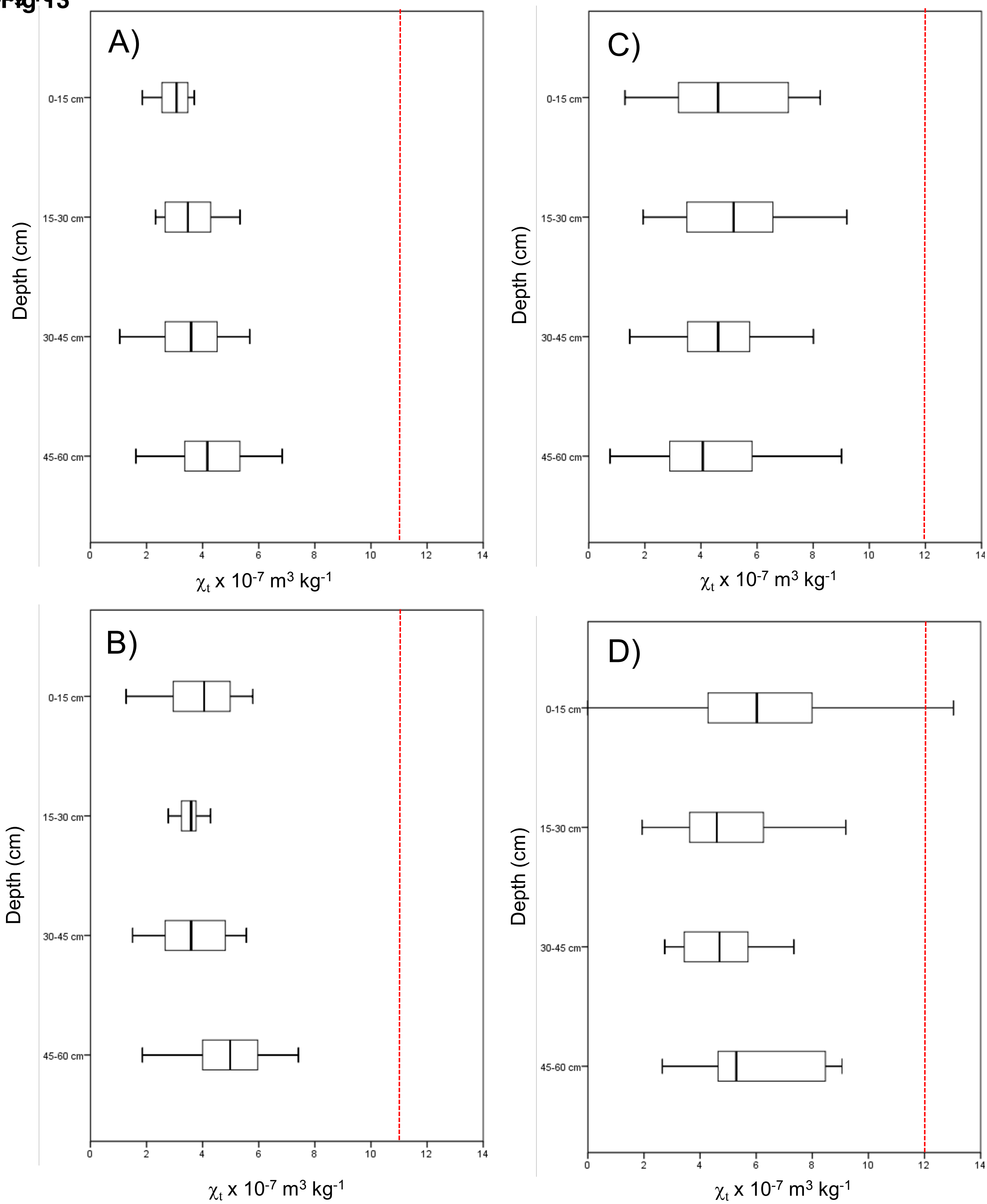

A)
B)
C)
D)
Depth (cm)
0-15 cm
15-30 cm
30-45 cm
45-60 cm
0
2
4
6
8
10
12
14
χ_t x 10^{-7} m^3 kg^{-1}

Fig 14

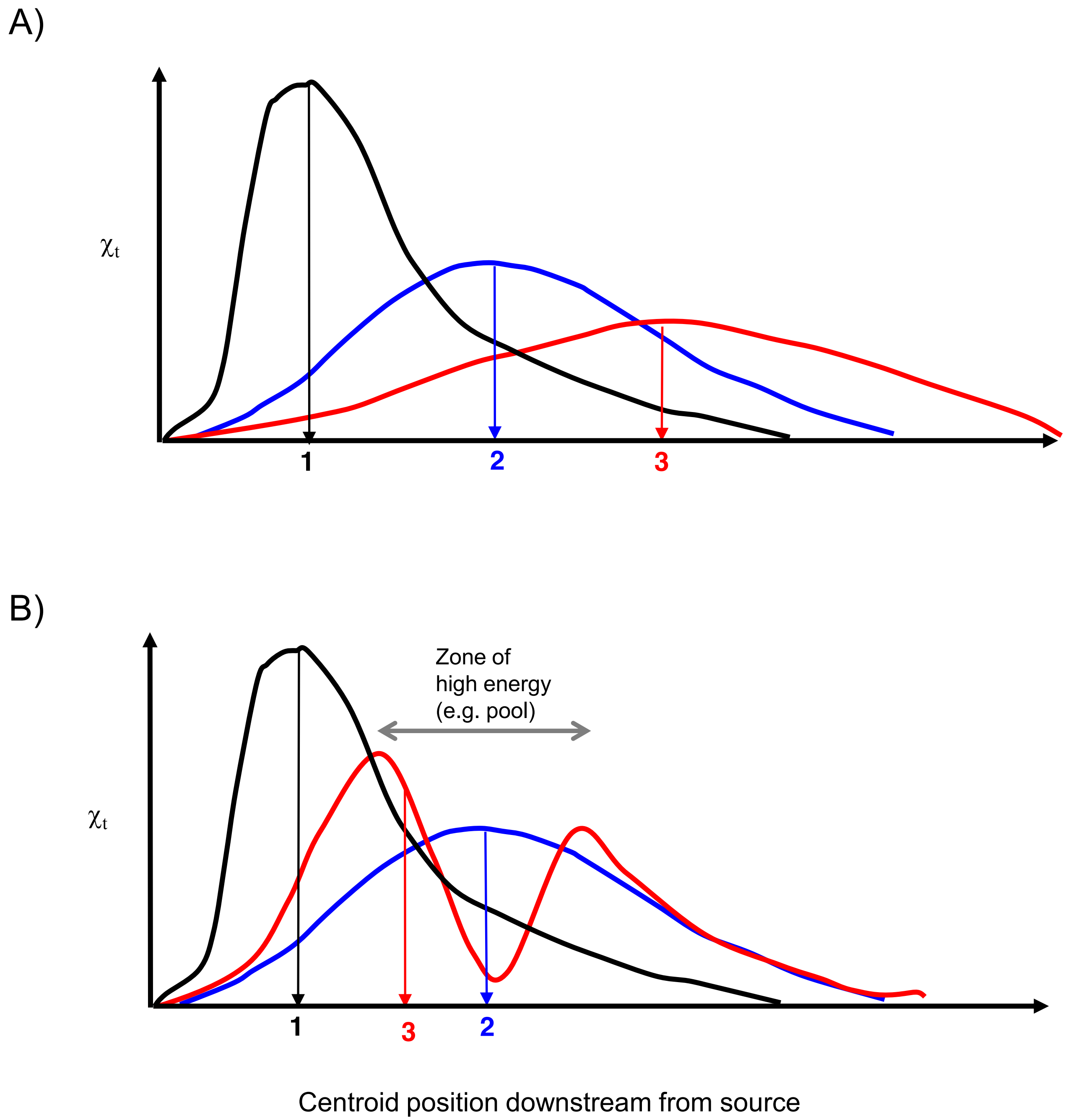
A)
χt
1
2
3
B)
Zone of
high energy
(e.g. pool)
χt
1
3
2
Centroid position downstream from source